

PAPER • OPEN ACCESS

Online detection of movement during natural and self-initiated reach-and-grasp actions from EEG signals

To cite this article: Joana Pereira *et al* 2021 *J. Neural Eng.* **18** 046095

View the [article online](#) for updates and enhancements.

You may also like

- [A state-based probabilistic method for decoding hand position during movement from ECoG signals in non-human primate](#)
Behraz Farrokhi and Abbas Erfanian
- [Individual finger control of a modular prosthetic limb using high-density electrocorticography in a human subject](#)
Guy Hotson, David P McMullen, Matthew S Fifer et al.
- [Estimation of the velocity and trajectory of three-dimensional reaching movements from non-invasive magnetoencephalography signals](#)
Hong Gi Yeom, June Sic Kim and Chun Kee Chung



PAPER

OPEN ACCESS

RECEIVED
15 January 2021

REVISED
26 May 2021

ACCEPTED FOR PUBLICATION
15 June 2021

PUBLISHED
2 July 2021

Original content from
this work may be used
under the terms of the
[Creative Commons
Attribution 4.0 licence](#).

Any further distribution
of this work must
maintain attribution to
the author(s) and the title
of the work, journal
citation and DOI.



Online detection of movement during natural and self-initiated reach-and-grasp actions from EEG signals

Joana Pereira , Reinmar Kobler , Patrick Ofner , Andreas Schwarz and Gernot R Müller-Putz*

Institute of Neural Engineering, Graz University of Technology, Graz, Austria

* Author to whom any correspondence should be addressed.

E-mail: gernot.mueller@tugraz.at

Keywords: brain–computer interface, movement detection, electroencephalography, reach-and-grasp, movement-related cortical potentials, low-frequency time-domain

Supplementary material for this article is available [online](#)

Abstract

Movement intention detection using electroencephalography (EEG) is a challenging but essential component of brain–computer interfaces (BCIs) for people with motor disabilities. *Objective.* The goal of this study is to develop a new experimental paradigm to perform asynchronous online detection of movement based on low-frequency time-domain EEG features, concretely on movement-related cortical potentials. The paradigm must be easily transferable to people without any residual upper-limb movement function and the BCI must be independent of upper-limb movement onset measurements and external cues. *Approach.* In a study with non-disabled participants, we evaluated a novel BCI paradigm to detect self-initiated reach-and-grasp movements. Two experimental conditions were involved. In one condition, participants performed reach-and-grasp movements to a target and simultaneously shifted their gaze towards it. In a control condition, participants solely shifted their gaze towards the target (oculomotor task). The participants freely decided when to initiate the tasks. After eye artefact correction, the EEG signals were time-locked to the saccade onset and the resulting amplitude features were exploited on a hierarchical classification approach to detect movement asynchronously. *Main results.* With regards to BCI performance, 54.1% (14.4% SD) of the movements were correctly identified, and all participants achieved a performance above chance-level (around 12%). An average of 21.5% (14.1% SD) of the oculomotor tasks were falsely detected as upper-limb movement. In an additional rest condition, 1.7 (1.6 SD) false positives per minute were measured. Through source imaging, movement information was mapped to sensorimotor, posterior parietal and occipital areas. *Significance.* We present a novel approach for movement detection using EEG signals which does not rely on upper-limb movement onset measurements or on the presentation of external cues. The participants' behaviour closely matches the natural behaviour during goal-directed reach-and-grasp movements, which also constitutes an advantage with respect to current BCI protocols.

1. Introduction

Movement has been studied over the years using electroencephalography (EEG) signals. EEG signals provide valuable information for basic neuroscience research on the neurophysiology behind movement initiation and preparation, as well as for applied research in the field of non-invasive brain–computer interfaces (BCIs) [1–3]. For the latter, the detection and discrimination of movement attempts can

be useful for people with motor impairments, such as spinal cord injury (SCI) or stroke. One of the goals is to detect and decode several movements and respective kinematic parameters from the EEG signals and translate them into commands to be executed by external devices like neuroprostheses [4–6], or robotic arms [7]. For instance, in a BCI control scenario for a grasp neuroprosthesis, the movement detector would continuously discriminate any grasp intention from rest. Once a grasp is detected, then the

movement decoder would classify the grasp type, e.g. palmar grasp vs. lateral grasp.

EEG neural correlates of movement manifest as oscillation-based activity [8] but also as activity in the low-frequency time-domain of the EEG. Interest in the low-frequency time-domain signals is reflected in several studies which aim to detect or decode upper-limb movements from movement-related cortical potentials (MRCPs). MRCPs are elicited during voluntary movements, and are usually revealed by locking the low-frequency EEG signals to the movement onset [9]. MRCPs consist of several sub-components: a first negative potential, the early readiness potential, which can start as early as 2 s before movement onset; the late readiness potential, which manifests as a steeper negative deflection around 0.4 s before movement; the motor potential which occurs very close to the movement onset; and the post-movement components preceding a return to baseline [10].

It has been shown that MRCPs allow decoding several types of discrete upper-limb movements [11–16], movement kinetics and kinematics like force and speed [12, 17–19], or even detect the presence of motor goals [20]. While the majority of these studies were performed in non-disabled populations which executed or even imagined [13, 21] movements, very recently it was shown that the discrimination of movements from MRCPs is possible on individuals with cervical SCI who performed movement attempts [22]. Despite the promising results, there are less than a handful of studies which succeeded in transferring the offline findings to a practical MRCPs-based BCI. To our view, one of the biggest obstacles of transferring a movement detector to a BCI application is the type of experimental paradigm used to gather calibration data for the detector.

First, for proper data labelling, it is necessary to accurately measure a movement onset. Most of the MRCPs-based offline/online detection studies have relied on electromyography (EMG) to obtain the onset of movement, in both healthy and stroke populations [23–27]. However, in a population without any residual upper-limb function, as can be the case in high SCI lesions, a movement onset is difficult, if not impossible, to measure. To solve this issue, participants often get asked to initiate the motor task after presentation of discrete visual or auditory ‘go cues’, i.e. the movements are externally-cued. While this allows for data labelling, there is an undesired overlap of response-evoked potentials, like the contingent negative variation (CNV) [28] observed in delayed-movement tasks, and therefore the features used for calibrating the detector differ substantially from those in a realistic scenario in which movements are self-initiated [29]. In [21], healthy participants memorized the number that was on a scroller at the time they felt the urge to initiate the imagination of a reach-and-grasp movement. With this strategy, it

was possible to achieve proper data labelling and a reasonable offline detection performance on a self-initiated task. However, the additional memorization task increased the cognitive load which could have altered the MRCPs characteristics [30] and further required a monitor for presentation of the scroller. In [22] and later in [31], other experimental paradigms were evaluated online which avoided the presentation of discrete cues but the movements were not self-initiated (on the calibration datasets).

Second, the experimental paradigms used so far do not allow shifting the gaze towards the movement goal and performing the motor task simultaneously. The reason is that saccades contaminate the EEG signals to an extent that they can mask the signal of interest [32, 33]. Researchers have tackled this issue by either not having a movement target; not allowing the participants to look at the target and asking them to fixate their gaze in a cross located in the centre of the field-of-view [24]; or by instructing the participants to first look at the target and only later perform the movement, as in [15].

In the present study we attempt to tackle these two main issues through an experimental paradigm which can be easily transferred to people without residual upper-limb movement function and also closely resembles the final BCI application. Twenty non-disabled participants initiated several reach-and-grasp actions at their pace, and to one of two targets. In one experimental condition, the participants could simultaneously shift their gaze to the target and reach-and-grasp it. In another condition, participants solely shifted their gaze towards the target. After correcting artefacts introduced by the gaze shifts, we assessed the differences on the low-frequency time-domain EEG signals among both conditions by time-locking to the saccade onset. Finally, we implemented a hierarchical classification approach to detect movement. This approach was evaluated online in both experimental conditions and additionally during rest.

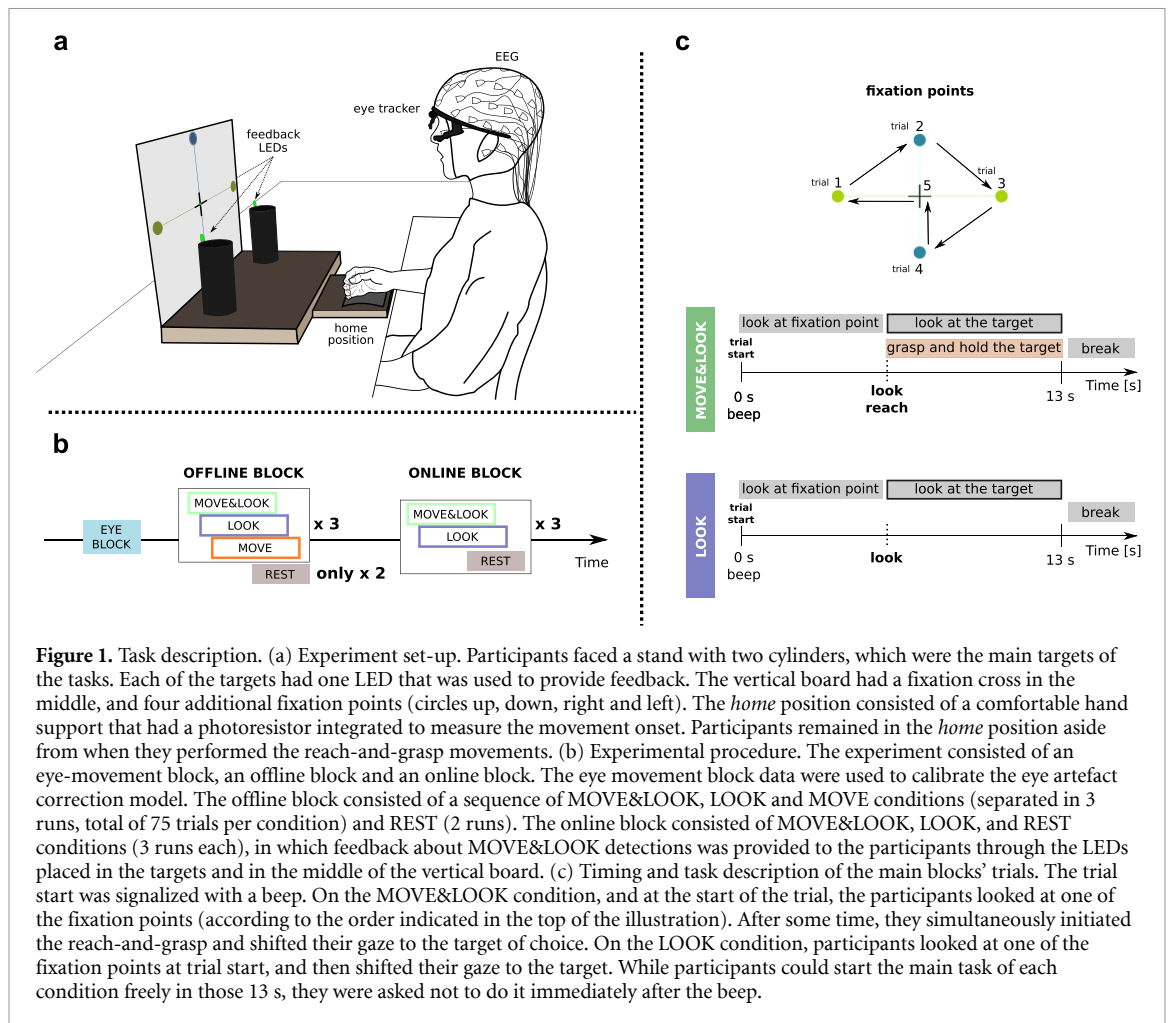
2. Materials and methods

2.1. Participants

Twenty non-disabled participants (25.6 ± 4.1 (mean \pm s.d.) years old, 7 male) took part in the experiment. Participants gave their informed consent and the study was conducted in accordance with the protocol approved by the ethics committee of the Medical University of Graz (approval number: 31-245 ex 18/19). All participants self-reported to be right-handed. Participants did not wear contact lenses or glasses. All participants received monetary compensation.

2.2. Instructions and task

Participants sat on a comfortable chair, facing two cylinders placed on a small stand (figure 1(a)). Whenever at rest, participants had their right hand



lying in the 'home' position, which was integrated on the stand. Photoresistors were placed below the home position and in the cylinders to record the movement onset and the grasp time-points, respectively. In the stand there was a vertical board with a fixation cross and four circles placed up, down, right and left with respect to the fixation cross. Two green LEDs were placed on each cylinder and one was placed in the middle of the vertical board. These LEDs were used to provide feedback to the participants with regards to the movements detected by the BCI in the online block of the experiment. We have decided to use LEDs instead of a robotic arm because the LEDs enabled us to provide a simple proof-of-concept of the online classifier, and the participants would not benefit from a robotic arm control as they were able to move their arms. Participants were asked to minimize blinks and muscular artefacts except during break periods, and we explained the negative effects of artefacts on the EEG recordings.

The experiment consisted of one eye movement block and two main blocks, as depicted in figure 1(b). The main blocks consisted of an *offline* block followed by an *online* block in which participants received feedback through the LEDs. Data recorded on the offline block were used to calibrate two classifiers which were later used in the online block.

On the offline block, four conditions were recorded: MOVE&LOOK, LOOK, MOVE, and REST. On the online block, three conditions were recorded: MOVE&LOOK, LOOK, and REST. We now describe the eye movement, the offline and the online blocks in detail.

2.2.1. Eye movement block

We recorded a block in which participants performed a series of eye artefacts in order to use the sparse generalized eye artefact subspace subtraction algorithm (SGEYESUB) described in [34] to correct the main blocks for eye movement artefacts and blinks. The paradigm was adapted from [34] to be more similar to the remaining main blocks, and therefore instead of displaying moving targets on a monitor, auditory cues were presented. The trial-based paradigm consisted of four conditions, namely REST, HORZ, VERT and BLINK. We recorded 10 trials for the REST condition, and 6 trials per HORZ/VERT/BLINK conditions. The conditions were randomly ordered. Each trial started with the auditory cue indicating the condition type, followed by an 11 s task and a short break of random duration between 3 and 3.5 s. On the REST condition, the participants were instructed to focus their gaze on the fixation cross and avoid blinking. On the HORZ/VERT conditions the participants moved

their eyes along the horizontal/vertical lines between the green/blue circles of the board (figure 1(a)). Participants were instructed to perform the eye movements smoothly and repeatedly, with a frequency that was previously trained according to a metronome beat (1 Hz, 60 bpm). On the BLINK condition, participants looked at the fixation cross and blinked repeatedly according to that same frequency.

2.2.2. Offline block

On the offline block four conditions were recorded: MOVE&LOOK, LOOK, MOVE, and REST. With the exception of the REST condition, we recorded 75 trials per condition, separated in 3 runs (25 trials per run). A beep sound marked the start of each trial, which was then followed by a 13 s task period. Breaks between trials were indicated with an audio cue, and had a duration of 1.5 s. The trials' timing and task descriptions are illustrated in figure 1(c) for each condition. The MOVE condition is not relevant for the present investigation and thus is not described hereafter.

On the MOVE&LOOK condition participants looked immediately after the beep at one of the fixation points on the vertical board (starting from the left green circle on trial 1, then blue upper circle on trial 2, and so on according to the order indicated in figure 1(c), top). Then, they could decide when to initiate the task, which consisted in shifting their gaze and reaching-and-grasping one of the targets of their choice. The movements were always performed with the right hand, and we instructed the participants to try to keep their target choice balanced. We asked the participants to initiate both the saccade and the arm movement simultaneously. They held and looked at the target till the break cue, and then returned to the home position. On the LOOK condition participants also looked at the different fixation points after the beep, and then freely decided when to shift their gaze to the target. They looked at the target till the break cue. In this condition, the participants always kept their hands on the *home* position. The goal of using different fixation points and presenting two targets was twofold. First, the paradigm becomes closer to a real-life scenario, in which the end-users can be looking at different points in the environment prior to the (attempted) movement. In a real-life scenario, there are also several possible targets, but only one is the motor goal. Second, the five fixation points and two targets cause various saccade directions and with them different eye dipole induced artefacts. This way, we reduced the risk that our linear classifier was relying on residual eye dipole artefacts, as they were varying from trial to trial. On the REST condition, the task duration was 11 s and we recorded 2 runs each with 12 trials. Participants were instructed to fixate their gaze at the cross and to avoid blinking or muscular artefacts.

2.2.3. Online block

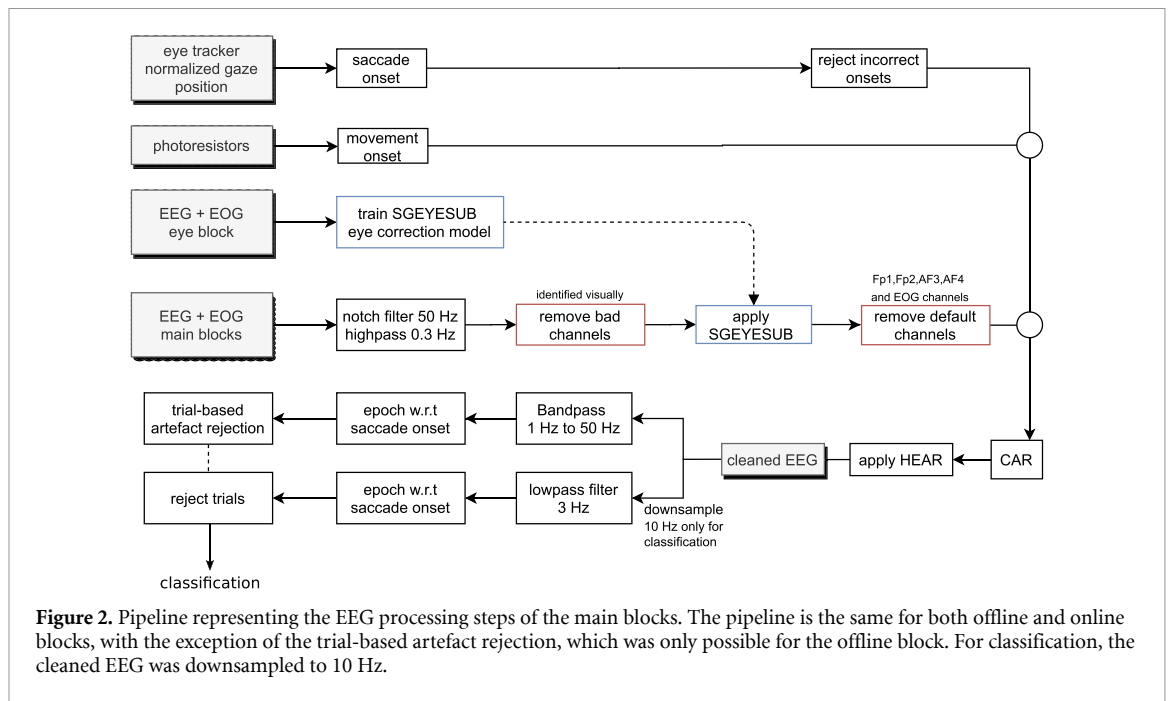
The trial structure and description of the online block is similar to that of the offline block. The only difference was that feedback about MOVE&LOOK detections was presented through the LEDs. On the MOVE&LOOK condition, if the MOVE&LOOK action was correctly detected by the classifier on the [0.5, 2.5] s time-window with respect to the saccade onset, the LED on the target would switch on for 1 s. On the LOOK condition, if the MOVE&LOOK action was wrongly detected by the classifier on the [0.5, 2.5] s time-window with respect to the saccade onset, the LED would also switch on. The limits of these [0.5, 2.5] s time-windows were defined based on our BCI evaluation procedure, which is explained in detail in section 2.5.4. In the case of the REST condition, we presented continuous feedback on false positives: the LED in the middle of the fixation cross would switch on if the MOVE&LOOK action was detected. We explained the meaning of the feedback to the participants. We recommend the reader to watch the supplementary video (available online at stacks.iop.org/JNE/18/046095/mmedia), through which it is possible to visualize the experimental setting and participant's actions during several online trials, and for all conditions.

2.3. Recordings

EEG and electrooculography (EOG) signals were recorded using 64 gel-based and active actiCAP electrodes (BrainProducts GmbH, Gilching, Germany). The reference electrode was placed on the left earlobe and ground on AFz. The EEG was measured from 61 channels placed according to the 10-10 system (channel layout can be seen in figure S1 of supplementary materials). Three EOG electrodes were placed above the nasion and below the outer canthi of the eyes. Biosignals were sampled at 200 Hz using two 32-channel BrainAmp amplifiers, and inspected using the BrainVision software (BrainProducts GmbH, Gilching, Germany). We used an ultrasound-based digitizer (ELPOS, Zebris Medical GmbH, Isny, Germany) to record the EEG electrode positions in 3D space. Gaze positions in normalized 2D coordinates were tracked using a Pupil Core eye tracker headset (PupilLabs, Berlin, Germany [35]). Three photoresistors were used to record the movement onset (at the home position), and the grasp onsets (one photoresistor placed on the right lateral side of each target). The sensor output was digitized using an Arduino microcontroller. For the recordings and time-synchronization we used the lab streaming layer (LSL) protocol (Swartz Center for Computational Neuroscience, UCSD).

2.4. Behavioural analysis

We analysed the behaviour of the participants during the main blocks. Depending on the condition, we investigated the time distribution of the saccade and



movement onsets with respect to the start of the trial; and the difference between saccade and movement onsets. Movement onsets were detected by thresholding the signal amplitudes recorded from the photoresistor placed at the home position. The saccade onsets were determined using the 2D gaze position estimated using the PupilCapture software (PupilLabs, Berlin, Germany [35]). Bad eye tracking data was removed prior to saccade detection, using the confidence value of each gaze position, also provided by the software. Then, offline data was epoched from [0, 13] s with respect to the trial start. Saccades were seen as outliers in 2D velocity space [36, 37]. The velocity thresholds for saccade detection were determined relative to the noise level of the data (which was calculated on the baseline period of [0.5, 1] s). All saccade detections were visually inspected and for both behavioural and EEG analysis we discarded trials in which the saccade onset was incorrect or not detected.

2.5. Signal processing

EEG and EOG were processed both offline and online using MATLAB 2017b (MathWorks Inc., Massachusetts, USA). We additionally used BioSig [38], EEGLAB [39] and Brainstorm toolboxes [40]. Signal processing steps are described in detail in the following sections.

2.5.1. Eye movement block

We started by applying a notch filter at 50 Hz to remove power line noise. Bad channels identified through visual inspection were removed. On average, 2.7 ± 2.0 bad channels were rejected per participant. Low-pass filtered EOG signals were used to extract the period of eye-movements and blinks from

the epoched data. Then, we fitted the sparse generalized eye subspace subtraction algorithm (SGEYESUB) as described in detail in [34]. This algorithm ensures minimal subspace activity during the rest periods, and has therefore shown to achieve a good trade-off between attenuating the eye artefacts while maintaining brain activity. Subsequently, the frontal channels Fp1, Fp2, AF3, and AF4 were excluded from further analysis, and common average reference (CAR) was applied. Finally, the high-variance electrode artefact removal (HEAR) model was calibrated on the REST epochs to later account for channel pops and low-frequency drifts, which can negatively affect the low-frequency EEG signals of interest [41]. This algorithm calculates the artefact-contamination probability individually for each channel based on a variance increase in the data compared to the calibration data. Then, it corrects the channel by interpolation based on the neighbouring channels. The interpolation is weighted using the aforementioned artefact-contamination probability.

2.5.2. Offline blocks

The processing pipeline for the offline block is outlined in figure 2. Data from all conditions were notch filtered at 50 Hz to remove power line noise. Then, a 2nd order high-pass Butterworth causal filter was applied at 0.3 Hz. Bad channels identified through visual inspection were removed. After correcting for eye movement artefacts, the most frontal channels were removed, and CAR was applied to the EEG signals. At this point, we applied the HEAR model. In the following sections, we refer to the EEG in the channel-space after these correction procedures as *cleaned EEG*.

To eliminate eventual remaining artefacts on the data, a trial-based artefact rejection procedure was additionally used. For that purpose, the cleaned EEG signals were first band-pass filtered from 1 to 50 Hz with a zero-phase 4th order Butterworth filter. Then the EEG was epoched with respect to the saccade onset (on the MOVE&LOOK and LOOK conditions) on a time-window of $[-2, 2]$ s. EEGLAB toolbox functions were then used to (1) find values outside an interval between -150 and $150 \mu\text{V}$, (2) reject trials with abnormal joint probability and/or (3) abnormal kurtosis. A threshold of four times the standard deviation was used for each statistic. These artefact-contaminated trials were marked for rejection.

To extract the relevant low-frequency EEG activity for classification, a causal, 2nd order, low-pass Butterworth filter at 3 Hz was applied to the *cleaned EEG*. We then downsampled the data to 10 Hz to reduce computational effort. The events corresponding to the trials marked for rejection were removed from the data.

2.5.3. Classification models

We used the downsampled low-frequency EEG signals of the offline block to train two classification models which were combined in a hierarchical manner. First, a classifier was used to discriminate the MOVE&LOOK from the REST condition, we call this model M1. Second, a classifier was used to discriminate the MOVE&LOOK from the LOOK condition, we call this model M2. The first classifier (MOVE&LOOK vs. REST) was used to continuously detect the MOVE&LOOK condition, and the second classifier (MOVE&LOOK vs. LOOK) was tested on each of those detections to confirm whether the reach-and-grasp movement was indeed present. Due to this dependency, we call this approach hierarchical, and its calibration is described in detail in the following paragraphs.

For both models, M1 and M2, we used shrinkage linear discriminant analysis (sLDA). sLDA is a method that has been extensively used for classification of event-related potentials [42, 43] and also for movement detection and classification of MRCPs [13, 15, 16, 20–22, 44]. The input features for both models consisted of the amplitudes of the low-frequency, downsampled, cleaned EEG on the $[0, 1]$ s time-window with respect to the saccade onset in the case of the MOVE&LOOK and LOOK classes. For the REST class, we extracted in a 50/50 ratio 1 s epochs from the MOVE&LOOK + LOOK trials (outside the action periods), and 1 s epochs from the REST block. We classified the EEG using on average 54.4 ± 2.0 channels at 11 time-points ($54 \text{ channels} \times 11 \text{ time-points} = 594 \text{ features}$). On average, there were 51 epochs per class. For each participant, the set of EEG features was divided into training and testing on a 5×5 -fold cross-validation procedure. In this procedure, the classifier performance was evaluated in

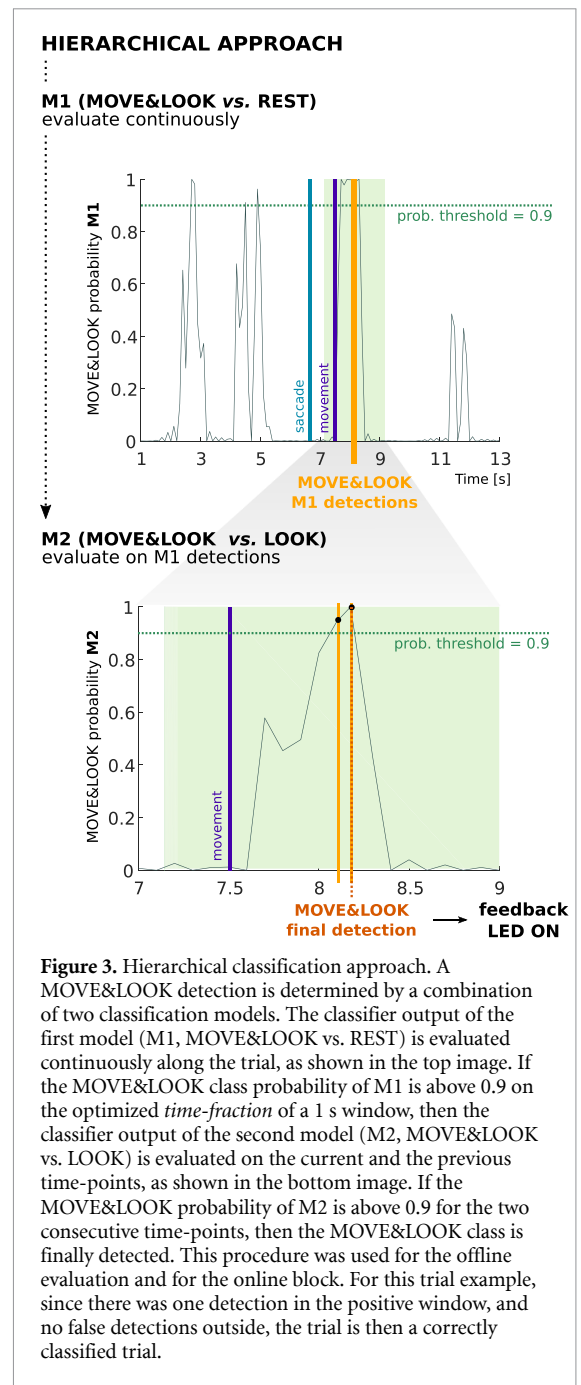


Figure 3. Hierarchical classification approach. A MOVE&LOOK detection is determined by a combination of two classification models. The classifier output of the first model (M1, MOVE&LOOK vs. REST) is evaluated continuously along the trial, as shown in the top image. If the MOVE&LOOK class probability of M1 is above 0.9 on the optimized *time-fraction* of a 1 s window, then the classifier output of the second model (M2, MOVE&LOOK vs. LOOK) is evaluated on the current and the previous time-points, as shown in the bottom image. If the MOVE&LOOK probability of M2 is above 0.9 for the two consecutive time-points, then the MOVE&LOOK class is finally detected. This procedure was used for the offline evaluation and for the online block. For this trial example, since there was one detection in the positive window, and no false detections outside, the trial is then a correctly classified trial.

an asynchronous manner that matched the online setting.

The hierarchical approach and its evaluation is exemplified in figure 3. The MOVE&LOOK vs. REST classifier output (M1) was continuously evaluated on the test folds with a sliding window of 1 s length, on every sample of each trial. This led to an evaluation period of 12 s per trial that corresponded to the trial length excluding its first second, which could be contaminated by an auditory-evoked potential. For the M1 model, we optimized a parameter which we call the *time-fraction*. This parameter corresponds to the fraction of the 1 s window which must be above or equal to a MOVE&LOOK class probability of 0.9 so that the MOVE&LOOK class is detected in M1.

The *time-fraction* varied between 0.1 and 1 with steps of 0.1. If the MOVE&LOOK was detected using the above criteria for M1, then M2 (MOVE&LOOK vs. LOOK classifier) was evaluated on the current sample and the previous sample. If the classifier probability of M2 was above 0.9 for the MOVE&LOOK class for two consecutive samples, then there was a final MOVE&LOOK detection. Details about the performance measure used for the optimization of the *time-fraction* are given in section 2.5.5. After finding the *time-fraction* parameter which maximized the performance of the hierarchical approach using cross-validation, we re-trained both M1 and M2 with all offline data. These were the final classifiers used in the online block. The activation patterns of the final classification models were calculated according to [45].

2.5.4. Online block

The online block consisted of MOVE&LOOK, LOOK and REST conditions, and was used to perform an online asynchronous evaluation of the movement detector. The data were preprocessed as already described for the offline block (figure 2(a)), excluding the trial-based artefact rejection step. We classified the EEG every 1/10 s (10 Hz) continuously on the [1, 13] s window with respect to the start of trial (beep sound). For each time-point, if the M1 MOVE&LOOK class probability was above 0.9 for the optimized *time-fraction* within the previous 1 s, then the output of the MOVE&LOOK vs. LOOK classifier (M2) was evaluated. Finally, if the MOVE&LOOK class of M2 was above 0.9 for two consecutive samples, then this corresponded to a final MOVE&LOOK detection.

On the MOVE&LOOK condition, we presented feedback of true positives: if MOVE&LOOK was detected on the [0.5, 2.5] s with respect to the saccade onset, then the target LED switched on for 1 s. On the LOOK condition, the target LED switched on for 1 s on false MOVE&LOOK detections on the [0.5, 2.5] s window with respect to the saccade onset. For simplification, we name the [0.5, 2.5] s windows, relative to the saccade onset, as the ‘action windows’ of the MOVE&LOOK and LOOK conditions. Generally, at an evaluation time-point t , the classifier output was evaluated using samples from the previous second, i.e. $[t-1, t]$ s. The lower limit of the action windows was set to half the length of that 1 s feature window (0.5 s). This ensured that at $t = 0.5$ s half of the samples used to evaluate the classifier output were already occurring after the saccade onset (at $t = 0.5$ s amplitudes are extracted from $[-0.5, 0.5]$ s). The upper limit of the action windows was less strictly defined, to account for eventual behavioural variability between performing the saccade and initiating the movement. We decided not to present continuous feedback on the classifier output, and to limit it to the action windows, to avoid distractions from the main task in the case of too many false positives. Continuous feedback

on false positives was provided only on the REST trials, in the [1, 11] s window with respect to the start of each trial. For those trials, the LED placed in the middle of the fixation cross switched on for 1 s in the case of a false positive detection. In all three conditions, there was a refractory period of 1 s after a detection.

2.5.5. Classifier performance

Several metrics were used to assess the classifier performance. A metric which has been used in asynchronous BCI evaluations [21, 26, 27, 46] is the percentage of correctly classified trials, which is a trial-based metric. In our case, a MOVE&LOOK trial is considered correct if there is at least one true positive on the MOVE&LOOK action window, and no detections outside. Figure 3 provides an example of such a correct trial. Since this measure integrates both information on FPs and TPs, it was chosen to evaluate the performance on the test folds of the offline block, in order to optimize the *time-fraction* parameter.

We additionally show the true positive rate (TPR) which represents the sensitivity of the detector, i.e. the percentage of MOVE&LOOK actions which were correctly detected. The positive window is the [0.5, 2.5] s action window of the MOVE&LOOK condition.

We also present three false positive measures. We calculated the false positives on the LOOK actions (FP_{look}), i.e. we show the percentage of LOOK actions which were wrongly identified as MOVE&LOOK. Here, the negative window is the [0.5, 2.5] s action window of the LOOK condition. The false positives were further calculated on the periods outside the action windows in both MOVE&LOOK or LOOK conditions (FP_{no_action}). These periods had an average duration of 25 min per participant, and we calculated the number of false positives per minute ($FP\ min^{-1}$). Lastly, we show the $FP\ min^{-1}$ on the pure REST trials (FP_{rest}). This evaluation period corresponded to ~ 5.5 min per participant.

We calculated the chance-level of each of these performance metrics on the online block by re-training the two classification models on the offline data with the classifier labels randomly permuted. We performed the permutation 500 times, and evaluated the performance of the hierarchical approach on the online data for each of these permutations [47, 48]. The optimal *time-fraction* parameter was used for evaluation of the classifier probabilities. The tails of each performance distribution were used to determine the significance boundaries: if the original performance was higher than the 95% percentile of the distribution established by randomly permuting the data, then the original performance was significant with $\alpha = 0.05$.

Finally, and for the sake of comparison, we also assessed the online detector performance if only the M1 model would have been used, thus eliminating the hierarchical approach.

2.5.6. EEG potentials

We analysed the EEG activity in the channel-space by applying the same processing as in figure 2 but replacing the filters by zero-phase filters. We then time-locked the trials to the points of interest, namely saccade and movement onsets. Trials were grouped according to the MOVE&LOOK and the LOOK conditions, separately per block type (either offline or online). After grouping in conditions, the mean and respective confidence interval ($\alpha = 0.05$, interval calculated using non-parametric t-percentile bootstrap statistics) for each condition per participant were calculated on a time-window between $[-1, 2]$ s with respect to the time-locking point. Group-level differences among the MOVE&LOOK and LOOK conditions were assessed on the time window of $[0, 1]$ s, at 11 time-points and with respect to the saccade onset. We used nonparametric paired-sample two-tailed permutation tests based on t -statistics ($\alpha = 0.05$). We accounted for multiple comparisons by calculating the permutation distribution using the maximum test statistic, t_{max} , over channels and time points. t_{max} denotes the most extreme positive or negative value of all the t -scores for each permutation [49, 50]. This analysis was done separately for the offline and online blocks. The electrodes which revealed a significant difference between conditions were plotted over the topographical maps representing the grand-average subtraction between the conditions: $\text{mean}(\text{MOVE\&LOOK}) - \text{mean}(\text{LOOK})$.

2.5.7. EEG source imaging

To better localize the sources of the EEG activity, we mapped the EEG signals of the online block to the cortical surface using the Brainstorm toolbox [40]. We computed the individual boundary element head models with OpenMEEG [51]. We used the ICBM152 brain model template and the participant-specific electrode locations. The registration between the ICBM152 template and the individual EEG electrode positions was done using the three anatomical landmarks (nasion, right and left preauricular points), and by projecting the electrodes to the scalp layer. The data from the REST runs was used to estimate the sensor noise-covariance matrices with shrinkage regularization [52]. To solve the inverse problem, we used sLORETA [53] with unconstrained dipole orientations, and obtained 15 002 cortical sources. The norm of the vectorial sum of the three orientations at each vertex was calculated and used to reveal the activity maps. To calculate the grand-average activity for each experimental condition, the participants' EEG activity was first normalized by its global field power (GFP) [54]. The global field power was estimated on the REST condition activity. To assess the difference between both MOVE&LOOK and LOOK conditions in the source space, we computed the significantly different voxels on a time-window of $[0, 1]$ s at 11 time-points with respect to the saccade

onset. We determined the significant voxels using paired-sample two-tailed permutation tests based on t -statistics ($\alpha = 0.05$, 5000 permutations, t_{max} used to correct for multiple comparisons [49, 50]). The EEG signals without the eye artefact correction were also mapped to the cortical surface using the same methodology, for both experimental conditions and their difference. This analysis was done in order to reveal the effect of applying the eye artefact correction method.

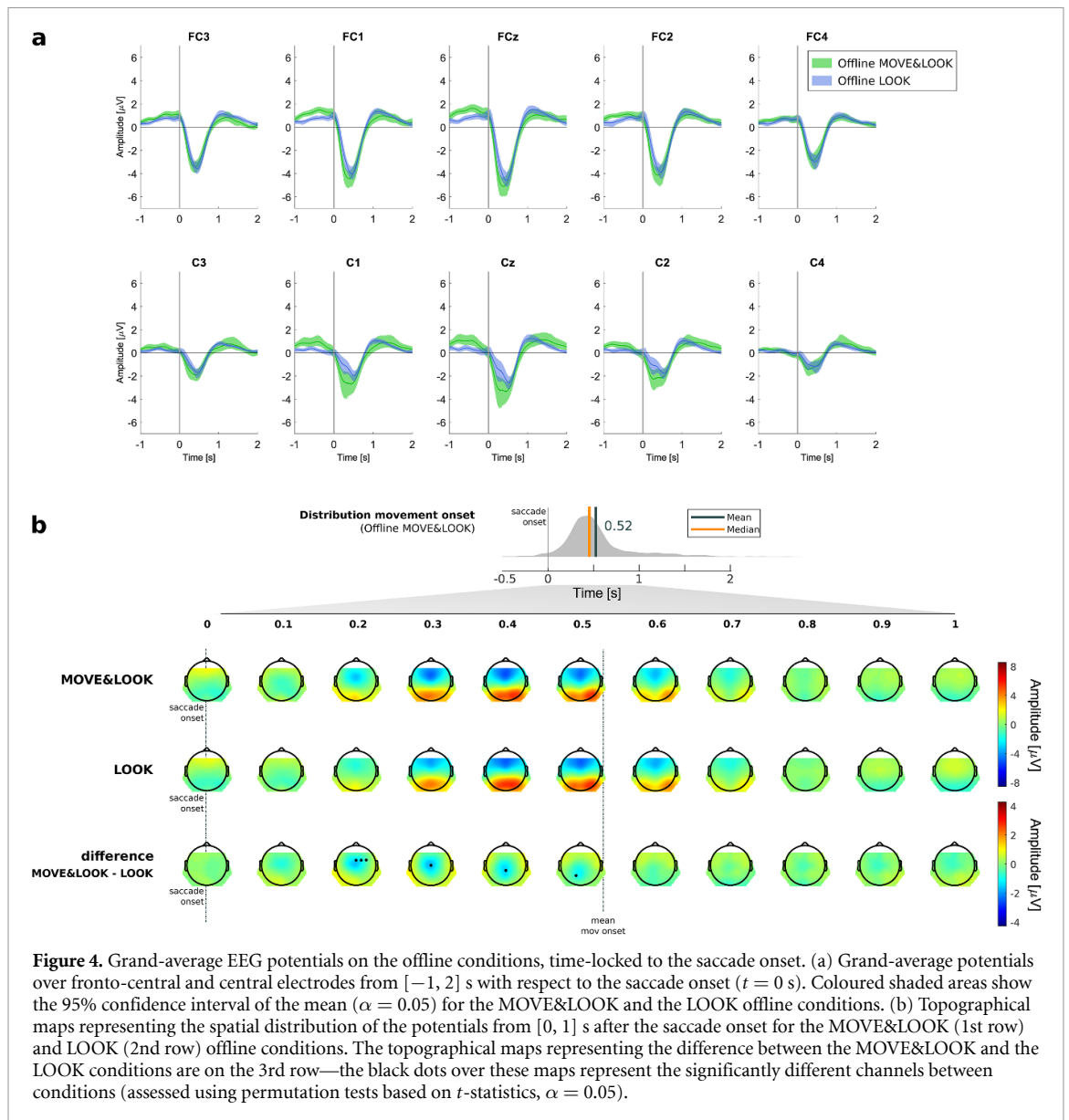
3. Results

3.1. EEG potentials

Figures 4 and 5 show the EEG potentials on the offline and online blocks of the experiment, respectively. Figures 4(a) and 5(a) show the time-course of the grand-average potentials for selected channels, aligned to the saccade onset ($t = 0$ s) and on a time window from $[-1, 2]$ s. Figures S2 and S3 of the supplementary materials show the grand-average potentials on a larger set of channels for the offline and online blocks, respectively. Figures 4(b) and 5(b) show the topographical maps corresponding to the time window from $[0, 1]$ s with respect to the saccade onset. The topographical maps are plotted per condition, and in addition the difference topoplots between MOVE&LOOK and the LOOK conditions are also shown. Over each difference topoplot we mark the electrode positions corresponding to the channels which showed statistically significant differences between both conditions.

Looking at the EEG potentials aligned to the saccade onset for the offline block (figure 4(a)), it is possible to observe that the activity before the saccade onset already reveals differences between MOVE&LOOK and LOOK conditions. Namely, the potentials associated with the MOVE&LOOK condition show a stronger amplitude for frontal channels when compared with the LOOK condition. After the saccade onset, both conditions reveal a fronto-central negativity, accompanied by a positivity in the occipital and parietal channels. The amplitude of the peak negativity on the fronto-central channels is stronger for the MOVE&LOOK condition ($-3.5 \mu\text{V}$ at 0.46 s, channel Cz) than for the LOOK condition ($-2.6 \mu\text{V}$ at 0.53 s, channel Cz). The potentials then return to baseline, fluctuating around $0 \mu\text{V}$ at 2 s after the saccade onset. The difference topoplots as well as the statistically significant channels marked on figure 4(b) confirm that there is a progression through time of the difference between the conditions: first the difference is most prominent at fronto-central electrodes, and then from 0.4 to 0.6 s mostly centro-parietal electrodes differ.

The EEG potentials on the online block (figures 5(a) and (b)) are very similar to the EEG potentials on the offline block, especially until the peak negativity. Again, the differences between



MOVE&LOOK and LOOK potentials are first manifesting over frontal-central channels and then progressing to parietal electrodes. However, around 1.6 s after the saccade onset, a stronger fronto-central positivity is observed for the MOVE&LOOK condition, when compared to the LOOK condition. The difference topoplots and the results of the statistical analysis in figure 5(b) also point out differences after the peak negativity, as potentials over the fronto-central channels were again significantly different between the conditions already 0.9 s after the saccade onset.

Figures S4 and S5 of the supplementary materials show the EEG potentials time-locked to the movement onset for the MOVE&LOOK condition in the offline and online blocks, respectively. Figure S6 of the supplementary materials represents those potentials as topographical maps.

To better localise the sources of the EEG activity in the time-window of $[0, 1]$ s with respect to the saccade onset, we have performed EEG source

imaging on the activity of the online block. This analysis was done for the EEG signals which were corrected for eye-movement artefacts (figure 6) but also without performing the artefact correction (supplementary materials, figure S7).

In figure 6, which corresponds to the eye-artefact corrected data, it is possible to observe that the EEG activity originates from the superior parietal cortex already at saccade onset, and for both MOVE&LOOK and LOOK conditions. The activity in both experimental conditions becomes stronger from 0.2 to 0.5 s after the saccade onset. Around that time window additional sources emerge from inferior parietal areas. Occipital areas are also active, but to a lesser extent when compared to the parietal activity. The significant differences between experimental conditions (bottom panel) originate from the primary motor cortex (M1), as well as premotor cortex and supplementary motor area (SMA), as it is possible to observe on the activity maps of the bottom panel

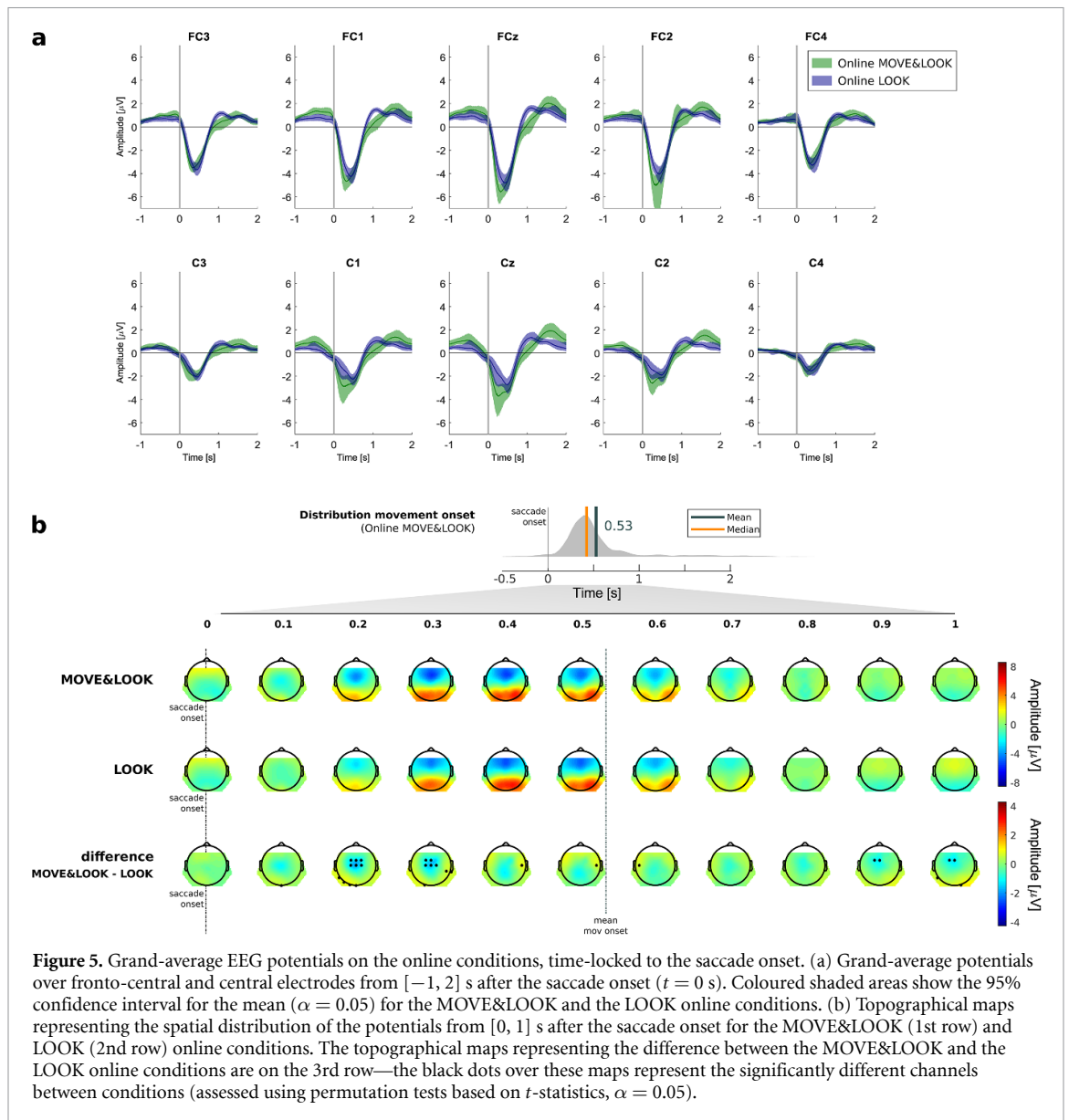


Figure 5. Grand-average EEG potentials on the online conditions, time-locked to the saccade onset. (a) Grand-average potentials over fronto-central and central electrodes from $[-1, 2]$ s after the saccade onset ($t = 0$ s). Coloured shaded areas show the 95% confidence interval for the mean ($\alpha = 0.05$) for the MOVE&LOOK and the LOOK online conditions. (b) Topographical maps representing the spatial distribution of the potentials from $[0, 1]$ s after the saccade onset for the MOVE&LOOK (1st row) and LOOK (2nd row) online conditions. The topographical maps representing the difference between the MOVE&LOOK and the LOOK online conditions are on the 3rd row—the black dots over these maps represent the significantly different channels between conditions (assessed using permutation tests based on t -statistics, $\alpha = 0.05$).

of figure 6. The activity in sensorimotor areas is significantly stronger for the MOVE&LOOK condition, when compared to the activity on the LOOK condition. Significant differences before but also during movement are additionally located in the occipital cortex, being once again the activity significantly stronger for the MOVE&LOOK condition.

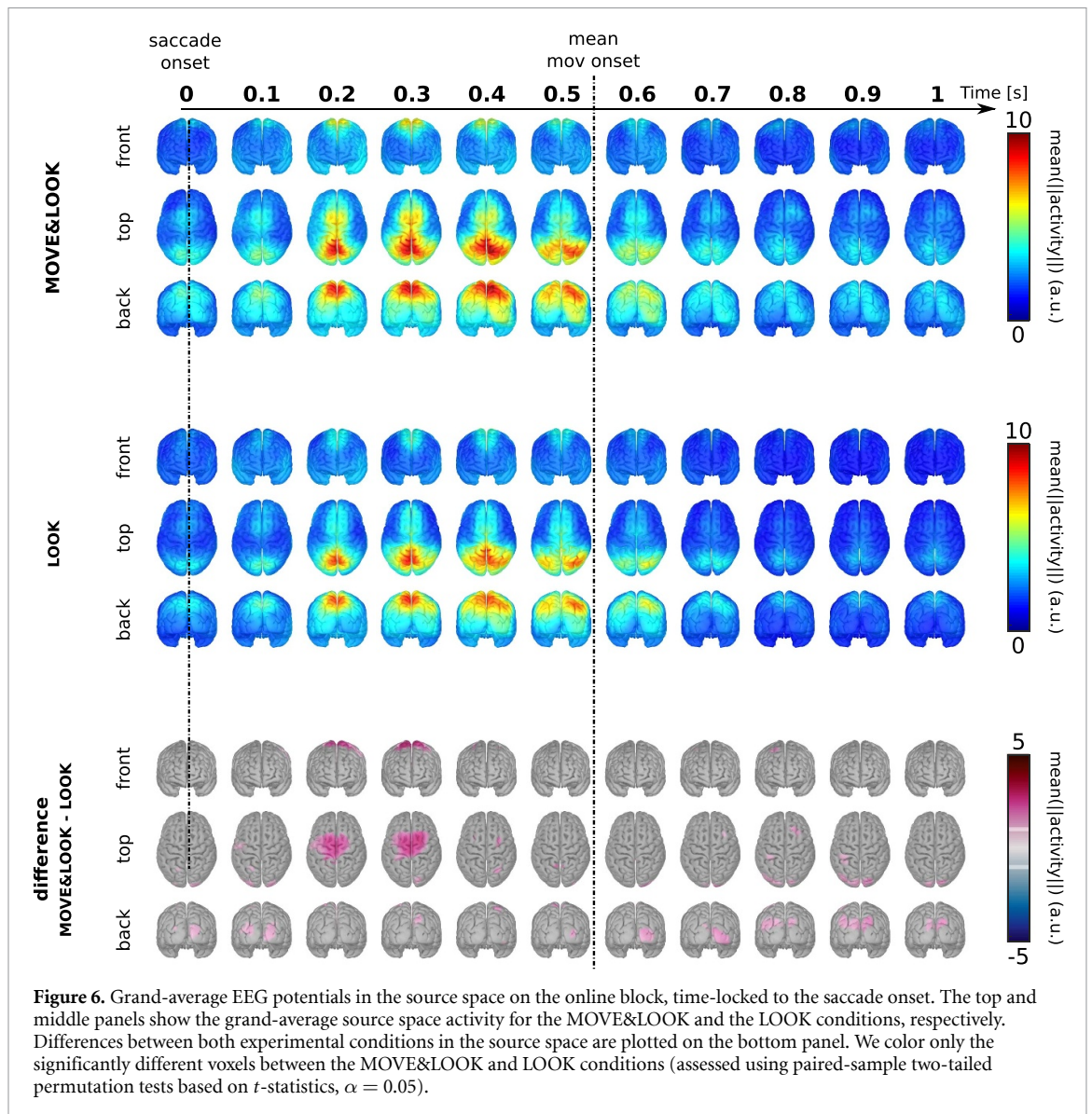
When analysing the results in the source space without the eye-artefact correction (figure S7), aside from the contributions of the sources identified in figure 6, there is also an additional strong prefrontal activity already at second 0, observed in both experimental conditions. The difference between conditions is again located in sensorimotor areas, as well as occipital cortex.

3.2. Classification results

3.2.1. Offline block

We used cross-validation to optimize a parameter which was relevant for the continuous evaluation

of the classifier output of M1 (MOVE&LOOK vs. REST). This parameter corresponds to the *time-fraction* of the 1 s window which must be above a class probability of 0.9 so that a detection occurs. On average, 0.6 (0.2 SD) of the 1 s window must have been above the 0.9 probability threshold for an optimal performance of the hierarchical model on the test folds. The participant-specific optimal values for the *time-fraction* parameter are listed in table 1 of the supplementary materials. The performance metric used to optimize this *time-fraction* was the number of correctly classified trials in the offline block; one trial was considered correct if there was at least one true positive within the MOVE&LOOK window of $[0.5, 2.5]$ s after the saccade onset, and no false positives outside that window. This metric allows the maximization of true positives while minimizing false positives. On average, on the test folds, 38.8% (6.7 SD) trials were correctly classified. The participant-specific performance on the offline block for the optimal *time-fraction*



values is shown in figure S9 of the supplementary materials. We then evaluated the detector's performance online.

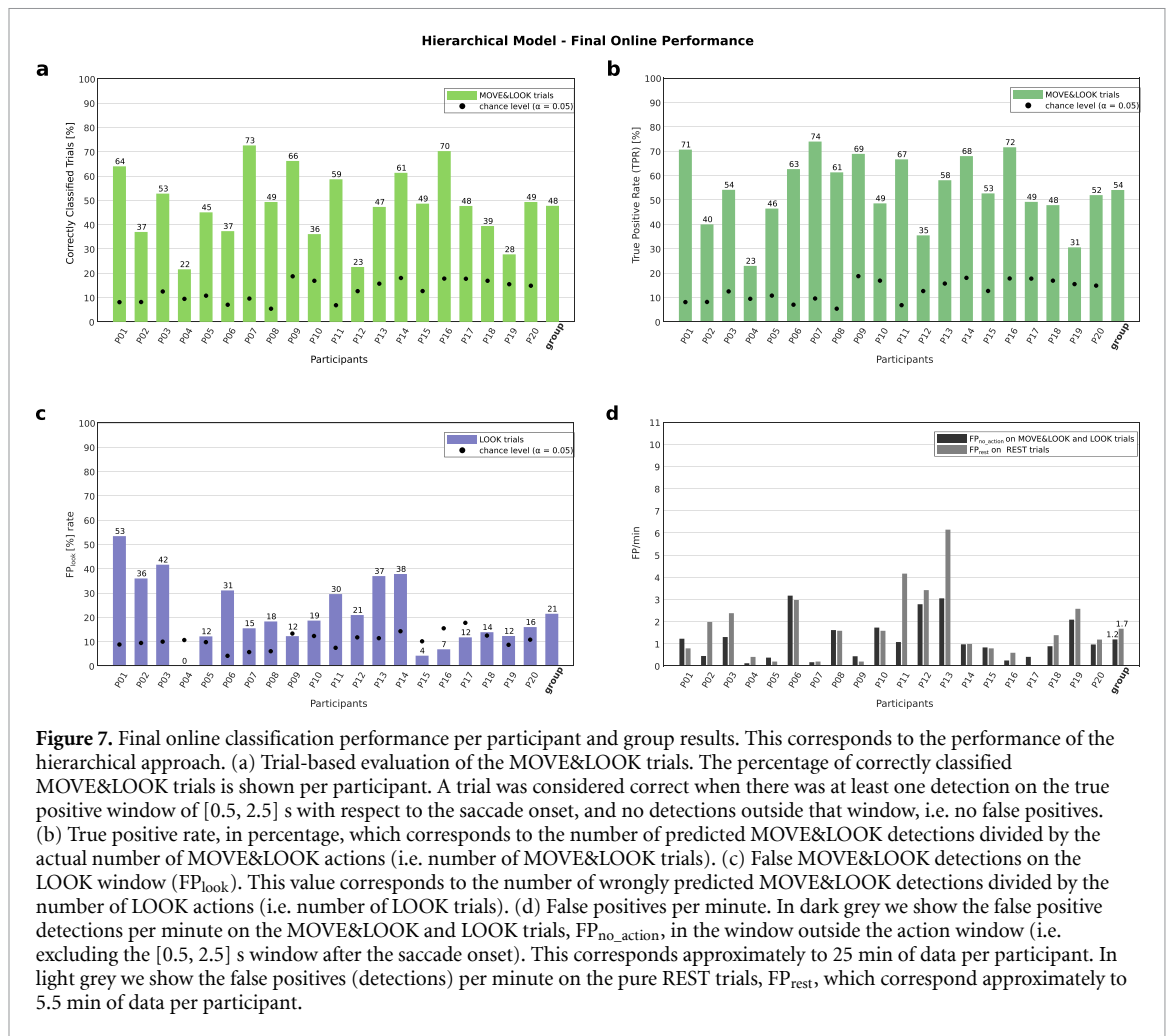
Figure S8 of the supplementary materials shows the average activation patterns for each final classification model, displayed as topographical maps. The patterns for M2 are very similar to the class-means difference observed in the difference topoplots of figure 5(b). Noteworthy, the activation patterns correspond to features extracted from causally-filtered data while the data in figure 5 were filtered with a zero-phase filter.

3.2.2. Online block

Figure 7 shows the final classification results, using the hierarchical model, on the online block. As in the offline block, we did a trial-based evaluation by calculating the percentage of correctly classified trials exclusively for the MOVE&LOOK online condition. The average percentage of correctly classified MOVE&LOOK trials was 47.8% (14.9% SD).

Chance-level is around 12.8% and the results for all participants were above chance-level. Figure 7(a) shows the individual results and respective chance-levels. A concrete example of this metric is provided for representative participant P08 on the online MOVE&LOOK trials (figure 8(b) top panel). For this participant, 49.3% trials were correctly classified.

The average true positive rate, which represents the percentage of MOVE&LOOK actions which were correctly identified as MOVE&LOOK, was 54.1% (14.4% SD). The TPR per participant and respective chance-levels are presented in figure 7(b). Individual rates were above chance-level for all participants. Figure 7(c) shows the false positive rate specifically on the LOOK actions, FP_{look} . On average, 21.5% (14.1% SD) LOOK actions were wrongly identified as MOVE&LOOK. The FP_{look} rate was at chance-level for 5 of the 20 participants, and the individual chance-levels were around 11%. Figure 7(d) focuses on $FP_{\text{no_action}}$ and FP_{rest} rates presented in false positives per minute ($FP \text{ min}^{-1}$). An average of

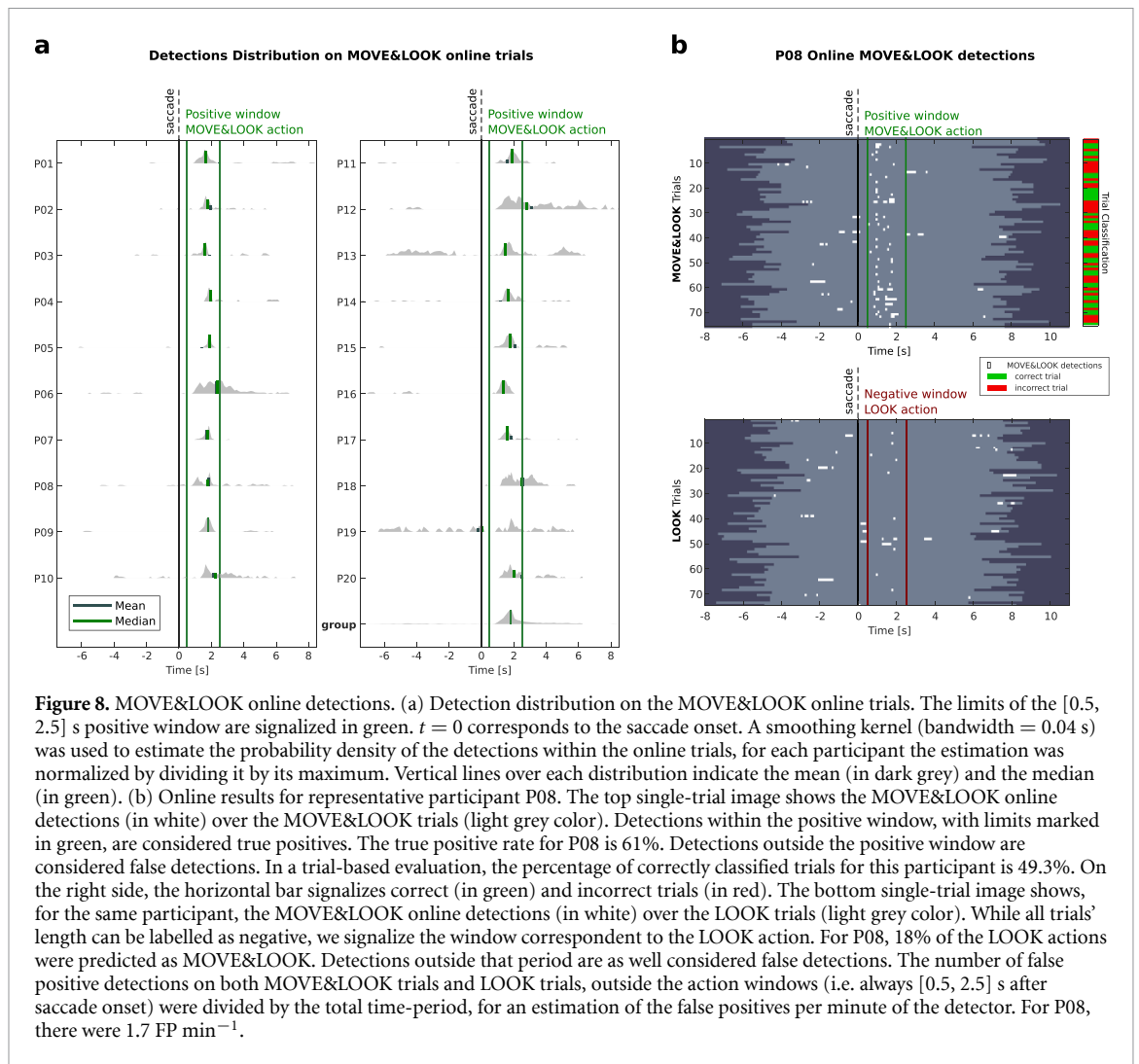


1.2 $FP_{no_action} \text{ min}^{-1}$ (0.9 SD) were detected in the MOVE&LOOK and LOOK trials outside the action windows, and an average of 1.7 $FP_{rest} \text{ min}^{-1}$ (1.6 SD) were detected in the REST trials.

It is also interesting to analyse the performance of the MOVE&LOOK detector when exclusively using the first classification model, M1, and thus eliminating the hierarchical approach. The average true positive rate was 70.5% (12.6% SD), which is larger than the TPR of the hierarchical model. However, the false positive rates also increase. On average, FP_{look} was 42.4% (21.0% SD). Furthermore, an average of 2.6 $FP_{no_action} \text{ min}^{-1}$ (1.8 SD) were detected in the MOVE&LOOK and LOOK trials and an average of 3.8 $FP_{rest} \text{ min}^{-1}$ (2.8 SD) were detected in the REST trials. Figure S10 of the supplementary materials presents the results for M1 at the individual level. Using the hierarchical approach, there is an overall decrease of false detections at the cost of fewer true detections. For a smaller group of participants, the hierarchical model presented an advantage. As an example, for participant P11, using M1 exclusively, the FP_{look} rate was almost as high (82%) as the TPR (85%). For this participant, the hierarchical approach led to a decrease of the TPR to 67%, but there was a much more noticeable drop of the FP_{look} rate to 30%.

Figure 8(a) shows the MOVE&LOOK detection distribution on the online MOVE&LOOK condition, for all participants and also at the group-level. We observe that the large majority of the detections happened within the positive action window, i.e. [0.5, 2.5] s. When looking at those correct detections, they occurred on average around 1.7 s (0.14 SD) after the saccade onset. This corresponds to 1.2 s (0.43 SD) after the measured movement onset. We also observe, as already expected from the above presented false positive rates, that there are detections outside the positive window.

Figure 8(b) shows the online detections for representative participant P08. The detections are plotted on single-trial images for both MOVE&LOOK (top panel) and for the LOOK conditions (bottom panel). First, it is evident that there are several MOVE&LOOK detections on the MOVE&LOOK window (limits highlighted in green). These correct detections are reflected in a true positive rate of 61%. Second, it is also evident that there are detections on the action period of the LOOK trials (bottom panel, window limits highlighted in red). They correspond to false detections, and result in 18% of LOOK actions being predicted as MOVE&LOOK. Thirdly, in both panels and outside the action windows, it is possible



to identify several false detections. For P08, these false detections resulted in 1.7 FP min^{-1} .

3.3. Behavioural results

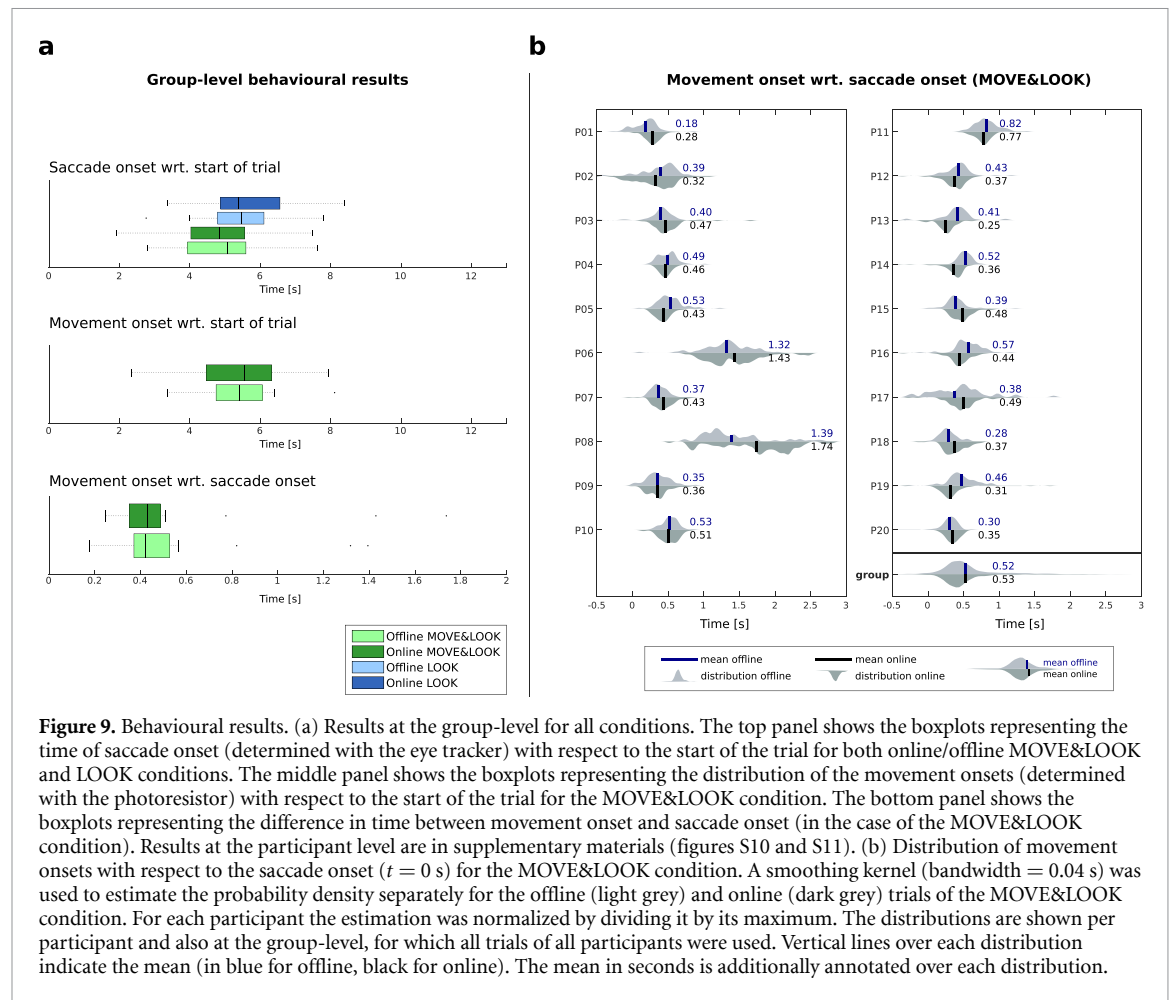
A summary of the behavioural results is presented in figure 9. The participant-level behavioural results are available at the supplementary materials (figures S11 and S12). Figure 9(a) shows a summary of the results at the group-level for all conditions from all blocks. We looked at the time-points of interest for each condition (start of trial, movement onset and saccade onset) and analysed their differences. With regards to the saccade onset, the boxplots in figure 9(a) (top panel) show that its distribution was spread over the trial duration and mostly from 2 s to 8 s after the start of trial. Similar results were obtained for the movement onset (figure 9(a) middle panel), detected using the photoresistor. Further, the boxplots represent similar distributions for both offline and online blocks, and both MOVE&LOOK and LOOK conditions.

Exclusively for the MOVE&LOOK condition, we could also analyse the time difference between moving and shifting the gaze to the target (figure 9(a)

bottom panel). At the group-level, and for the MOVE&LOOK offline trials, participants initiated their reach towards the target on average 0.52 s (0.31 s SD) after the saccade. For the online trials, very similar reaction times were observed: the mean movement onset with respect to the saccade onset occurred at 0.53 s (0.31 s SD). The distributions at the level of individual participants (figure 9(b)) reveal that all participants were, on average, initiating the movement after the saccade. The large majority of participants was able to keep a consistent behaviour from the offline to online blocks. It is also evident that there were two outliers, P06 and P08, that initiated their movement on average much later than the rest of the group. Their distributions are also more spread out.

4. Discussion

In this study we present a novel experimental paradigm for online and asynchronous detection of self-initiated reach-and-grasp tasks. In two experimental conditions, participants were asked to exclusively shift their gaze to the target (LOOK condition)



or to reach-and-grasp the target while simultaneously shifting their gaze towards it (MOVE&LOOK condition). By time-locking to the saccade onset, we were able to reveal the differences in the low-frequency time-domain of the EEG between both conditions, which were mainly located in sensorimotor areas. These differences, along with additional activity in the parietal and occipital areas, were exploited in a hierarchical approach which first discriminated MOVE&LOOK vs. REST, and only then discriminated MOVE&LOOK from LOOK. We tested the movement detector performance online in both experimental conditions, and additionally during rest. In this section we discuss the main results, highlighting their contribution to the development of BCIs for people with high SCI, without forgetting the current limitations.

4.1. Experimental paradigm

Experimental paradigms for BCIs, and movement detection in particular, often do not allow for ecological validity. The main reason is that the users are asked, specifically on the training blocks of the paradigms, to perform the tasks under very well-defined and strict rules. These rules allow for a better control of confounders and an accurate time and phase-locking which is important for the extraction of movement-related features. Nevertheless, they also

limit the transfer of the findings to real-world situations. Participants are typically required to react to visual or auditory cues, and the movements are not self-initiated. Specifically for movement detection or discrimination, this imposes a mismatch in the electrophysiological signals of interest between the training paradigm and the online application, in which movements are self-initiated [29].

In this study, we have designed a paradigm which aims to be closer to a real world situation and also easily transferable to people with SCI. We eliminated the presentation of visual or auditory 'go' cues, and allowed the participants to decide when to initiate the movement to real (i.e. no abstract or virtual) targets. The participants were instructed to look at the self-chosen target—departing from one of several possible fixation points—at the same time they initiated the goal-directed reach-and-grasp movement. We believe that this strategy is less restrictive and more natural than asking the participants to always fixate their gaze on a cross positioned in the environment. The saccade onset additionally served as a locking point, replacing the need of a movement onset (which is not possible to obtain in high SCI without residual upper limb function) or the need of 'go' cues. Even so, the additional oculomotor task also imposes other constraints in the generalization capabilities of the movement detector. These will be discussed in the next sections.

4.2. Participants behaviour

The analysis performed with regards to the participants' behavioural responses confirms that the participants were performing the tasks in a self-paced manner since the saccades were detected in very spread time-points with respect to the start of the trial (mostly ranging between 2 and 8 s after the trial start). Similar distributions were observed for both offline and online blocks of the experiment.

For the MOVE&LOOK condition, despite the instruction to perform the gaze shift simultaneously to the start of the reach-and-grasp, we expected that the participants would naturally—in a matter of milliseconds—first shift their gaze towards the target and then reach it [55]. On average, participants' movement onset was detected 0.52 s after the saccade onset. It is important to note that an EMG onset would provide an earlier onset than that of the photoreistor, thus reducing this difference. For 17 of the 20 participants, the time difference between the saccade and the reach was below 0.6 s. There are two clear outliers for which the mean difference is around 1.3 s. For those outliers, also the movement onset distribution was more spread than for the remaining participants. Similar distributions of movement onset with respect to the saccade onset were obtained for both offline and online blocks of the experiment.

4.3. EEG potentials

We used the saccade onsets as time-locking points to reveal the low-frequency time-domain EEG signals for the two conditions in both offline and online blocks. For the MOVE&LOOK condition we additionally time-locked the EEG to the detected movement onset.

On the offline block we observe in both conditions a clear fronto-central negativity, significantly stronger for the MOVE&LOOK condition, which peaks at 0.46 s after the saccade onset (and around 0.06 s before the average detected movement onset). Through source imaging, we could localise this activity to primary motor, premotor and supplementary motor areas. We attribute the strongest difference in EEG activity between both conditions to the reach-and-grasp movement initiation, which is only present in the MOVE&LOOK condition. The difference topoplots in figure 4(b), as well as the source maps in figure 6 reveal a potential which is identical in timing and spatial distribution to the MRCPs. The primary sensorimotor, the medial frontocentral, and premotor areas were pointed out as likely generators of the scalp-recorded MRCPs in [56]. Recently, Kobler and colleagues [44] investigated the EEG in the delta-band during a visuomotor task which involved externally-cued centre-out reaching movements. This task was compared to an oculomotor task in which participants did not perform the reaching movement but still tracked a target cursor on a monitor. They showed that central

sensorimotor areas were as well active on the oculomotor task (which required no arm movement), but they were active to a significantly weaker extent than in the visuomotor task. The weaker, but noticeable, activation of central sensorimotor areas in the oculomotor task found in [44] support our results, despite the substantial differences between the motor tasks involved. We have not observed a strong lateralization effect in the MOVE&LOOK condition or in the difference topoplots in figure 4(b): the peak-negativity in C1 was only slightly larger than the peak in channel C2. This was also the case in the results recently reported in [44]. For reaching movements, more proximal movements from the shoulder and eventually the trunk are necessary. Stancák *et al* have shown that MRCPs components preceding movement onset are largest over SMA regions for proximal movements, when compared to individual hand and finger movements [57]. Additionally, Jankelowitz *et al* have reported that potentials associated with self-paced movements are actually largest in mid-line areas, even for more distal movements [29]. While the weaker lateralization might be explained by the type and variability of the self-paced and dynamic reach-and-grasp movements executed in this study, this is a point which deserves future investigation and would additionally benefit from a more accurate time-locking (e.g. movement onset obtained with EMG).

Superimposed to the fronto-central negativity, we observed, in the channel-space, a positive potential in the parietal and occipital electrodes in both experimental conditions. This additional activity is most likely related with the oculomotor task present in both conditions, and the additional target selection task. Through source imaging, we show that this activity originates from superior parietal and inferior parietal areas, being occipital areas also active but to a lesser extent. It is well known that the posterior parietal cortex (PPC) plays an important role in integrating sensory information for movement planning [58–63]. Subregions of the parietal cortex are responsible for planning of several movement types, from saccades to hand movements [64, 65]. The PPC also plays a role in target selection during spatially guided movements. For instance, using spiking activity, Scherberger and Andersen have shown that target selection signals could be predicted from the PPC, when monkeys had to select one of two visual stimuli as target for either reach or saccade movements [66]. In [21], using the low-frequency time-domain of the EEG and source imaging, parietal areas were also found to encode differences between internally-driven target selection and externally-cued processes. Therefore, we attribute the parietal activity observed in the present study to visual guidance necessary for saccade/arm movement planning, and also to target selection processes. As a next step, it would be interesting to assess whether this activity would still be

present (and if, to which extent), when the oculomotor task is dissociated, or irrelevant, for the reaching task—i.e. if the eye movements would not have been goal-directed.

Interestingly, the results obtained in the source space additionally point to significant differences between experimental conditions in occipital regions, suggesting the involvement of visual areas in the encoding of effector information. Our findings corroborate with the results recently reported in [67]. Through three separate functional magnetic resonance imaging studies, Gallivan and colleagues report that activity in the early visual cortex is selectively modulated by goal-directed movement planning. Concretely, there was an effector-specific modulation, allowing to decode arm vs. eye movements, thus further supporting the idea that the visual cortex also sustains higher-level cognitive operations [68].

The EEG potentials observed on the online block are similar to the potentials observed on the offline block, with the exception of the time-period around feedback presentation. Feedback was presented on average around 1.7 s after the saccade onset on the online block. However, even before this time point we observed differences between the two experimental conditions. For instance, around 1.6 s after the saccade onset, we observe a stronger fronto-central positivity in the MOVE&LOOK condition, when compared to the LOOK condition. We attribute this difference to the presence of feedback. First, the participants were expecting that the LED would switch on after the saccade onset exclusively for the MOVE&LOOK condition. Second, the movements were detected more often in the MOVE&LOOK condition than in the LOOK condition, causing the LED to switch on 2.5 times more often. Both expectation and feedback presentation effects are likely responsible for the difference between experimental conditions on the online block.

Finally, by instructing the participants to perform saccades and reach-and-grasp movements, we have imposed a task which can originate eye and muscular artefacts. These contaminate the EEG signals, especially in the low-frequency range here investigated. With regards to muscular artefacts, we have not observed activity in temporal sites which could have corresponded to shoulder and neck movements. Moreover, we adjusted the board position for each participant, so that the targets would be in a comfortable reach distance. We performed eye artefact correction, offline and online, using a state-of-the-art correction algorithm which has been systematically assessed for low-frequency time-domain EEG signals, including MRCPs [34]. Signals before eye artefact correction were indeed contaminated with corneo-retinal dipole artefacts, time-locked to the saccade, which manifested in the source space through activity on areas closest to the eyes. We have removed this contribution, and show through source imaging that

the activity after eye artefact correction is not originating from prefrontal or anterior temporal areas.

4.4. Movement detection

We used the EEG potentials on the low-frequency time-domain to detect movement using a hierarchical approach that consisted of two classification models: M1 which classified continuously MOVE&LOOK vs. REST, and M2 which classified MOVE&LOOK vs. LOOK only after a detection on M1.

In the previous section, we have discussed our findings from a neurophysiology perspective which is fundamental when interpreting and discussing the performance of the movement detector. The oculomotor task in both experimental conditions led to a strong activity originating from the parietal and occipital cortices. Additional to this activity, central sensorimotor areas were also active, and to a stronger extent in the MOVE&LOOK condition. This activity corresponds to the MRCPs, typically observed around movement onset. The training features of the classifier models were extracted on a time-window from [0, 1] s with respect to the saccade onset, which covered mainly activity in parietal, occipital and sensorimotor areas. Concretely, for the first classifier, M1, activity was exploited from parietal, occipital, and fronto-central areas. For the second classifier, the discriminant activity was originating mainly from central areas, as can also be seen from the classifier's activation patterns in figure S8 of the supplementary materials (available online at stacks.iop.org/JNE/18/046095/mmedia). Overall, the movement detector was not only MRCPs-based, and our approach additionally exploited activity in the low-frequency time-domain originating from parietal and occipital sites. This represents a novelty in terms of movement detection from EEG in the low-frequency. While we cannot ensure generalization to movements which are not coupled to similar oculomotor tasks, we consider that our approach is more intuitive than others in which participants are not allowed to look at the movement targets.

The performance of the movement detector was evaluated on the online block through several performance metrics. We obtained an average true positive rate of 54%, and all participants were above chance-level performance. This means, an average of 54% of the MOVE&LOOK actions were correctly detected as MOVE&LOOK. On the LOOK online condition, an average of 21.5% LOOK actions were falsely detected as MOVE&LOOK. This value was at chance-level only for 5 out of 20 participants. With regards to false positives per minute, there were on average 1.2 FP min^{-1} in the LOOK and MOVE&LOOK conditions, outside the action windows. On the pure rest data, there were 1.7 FP min^{-1} . Translating the 21.5% FPR on the LOOK action windows to FP min^{-1} , this corresponds to an average of 5.4 FP min^{-1} , which is substantially higher than

the FP min^{-1} detected during the windows in which the participants were at rest. This indicates that the presence of an oculomotor task increases the chance that the movement detector falsely detects movement. Nevertheless, the FPR on the LOOK actions is also substantially lower than the TPR on the MOVE&LOOK actions.

Comparing the performance results here obtained with other studies using low-frequency time-domain EEG features is important. However, it is necessary to note that factors like the movement type, presence of visual cues, or even whether movement initiation was externally-cued or self-initiated can deeply affect the performance of the movement detectors. The online detection of movement using the EEG delta-band has been reported in lower-limb self-initiated movements in healthy populations. In these studies, EMG was recorded to determine the movement onset and extract the relevant features [25, 69]. True-positive rates of 67.15% in [69] and 79% in [25] were obtained. These performances are higher than the performance obtained by our detector, which can be explained by the more pronounced potentials typically observed in lower-limb movement tasks [70]. With regards to false positives, in [25], a rate of 1.4 FP min^{-1} were reported, which is equiparable to our results. For upper-limb movements most evaluations of the detectors' performance were done offline. A TPR of 76% was reported during execution of self-initiated reaching-tasks [24], and a TPR of 75% was obtained in cue-based protocols [71, 72]. First steps in online upper-limb movement detection and decoding have been recently done in [22] in a single-case study on a person with a complete cervical SCI. It was shown that an intact spinal cord was not necessary to detect and classify movements from the EEG. The movement detector obtained a TPR of 30% with more than 3 FP min^{-1} , a substantially worse performance, but again the experimental protocol and especially the population are not comparable.

Despite the false positives per minute in our study being in the range of those reported in the literature, it is important to discuss possible reasons for such spurious detections. In an asynchronous BCI scenario, a wide range of activity must be correctly detected as 'non-intentional' or as rest. This is a really challenging classification scenario, also because the participants are not completely inactive or 'free of thoughts' while at rest. Specifically for MRCPs, it has been shown that MRCP-like components might precede voluntary motor inhibition (e.g. when participants actively think of not moving) [10], and that activity building up to 200 ms before an actual movement onset might still be actively interrupted by the participant, preventing an overt movement [73]. Unfortunately, it is not possible to evaluate whether some of the false detections in our study are explained by such phenomena due to the lack of a ground truth.

We do identify a specific limitation in our classification method which could impact our results, specially for the discrimination between MOVE&LOOK and LOOK conditions. We have used a fixed time window to extract the features for calibration, which might not be optimal for each participant. In the future, it could be beneficial to optimize this window for classification of MOVE&LOOK vs. LOOK conditions. Such optimization could help to improve the performance of the classifier.

Another metric often used in trial-based evaluations is the percentage of correctly classified trials. In our study, a trial was correct if there was at least one detection on the positive window, and no detections outside. We have achieved 48% (15% SD) of correctly classified trials. In [21] a similar performance of 53% (17% SD) in a self-initiated movement imagination task was obtained. Additionally, in [26], on a healthy population performing seven types of self-initiated upper-limb movements, detection performance varied from 40% to 75% correctly classified trials, depending on movement type. In our study, we had a single task type. One of the questions that still remains to be answered is then how would our movement detector generalize to other types of upper-limb movements.

Correct detections happened on average 1.7 s (0.14 SD) after the saccade onset, or 1.2 s (0.43 SD) after movement onset. This difference in variability shows that the detections were more time-locked to the saccade onset, than to the movement onset. With regards to the latency of detections, it is important to mention that such detection latencies would not work for neuromodulation applications, since the delay between the intention of action and the feedback is in fact too big to induce plasticity [69]. In our study, the large latencies are not only caused by filtering or the length of the feature window itself, but also by the final detection logic. In our detection logic, and for the first classifier M1, a participant-dependent and optimized time-fraction of the 1 s sliding window must have been above a MOVE&LOOK class probability of 0.9. This contributes to a reduction of false positives and, in end-users with high SCI and for the control of a robotic arm or neuroprostheses, we believe that this reduction in false positives can be prioritized at the cost of later—but meaningful—detections.

We also analysed the performance of the detector when exclusively using the first classification model, M1. The average true positive rate was 70.5%, which is larger than in the hierarchical model by 16%. However, the false positive rates also increase. On average, 42.4% LOOK actions were wrongly identified as MOVE&LOOK (increase of 21%). Furthermore, an average of 2.6 FP min^{-1} were detected in the MOVE&LOOK and LOOK conditions (excluding the action windows) and an average of 3.8 FP min^{-1} were detected in the pure rest trials. Aside from an overall

decrease of false detections at the cost of fewer true detections, for a smaller group of participants, the hierarchical model presented a clear advantage. For those participants, there was a much more noticeable drop for the FPR on the LOOK action window than for the TPR on the MOVE&LOOK window. This meant that with the hierarchical approach the MOVE&LOOK and LOOK action windows were better separable. To our view, decisions on whether to use M1 alone or opting for the hierarchical approach must be seen individually according to the baseline (M1) performance or desired TPR/FPR ratio. A clear disadvantage for the hierarchical approach is that it requires more training data (i.e. an additional LOOK class) and for transfer to end-users this factor should be even more carefully considered. Nevertheless, it is still extremely important to evaluate how sensitive the detector is to saccades.

4.5. Future work

We have developed an experimental paradigm which is easily transferable to the SCI population and mimics a more realistic BCI scenario, allowing the participants to look at real targets. The task is intuitive and would involve, in the case of SCI, self-initiated upper-limb movement attempts. In first stages, movement detection feedback could still be given via the LEDs placed on the targets. Later on, more meaningful feedback should be presented, such as triggering movement through a grasp neuroprosthesis, or a robotic arm. However, before testing our movement detector in a SCI population, there are some considerations to be done. For instance, we consider it important to reduce the length of the experimental protocol and particularly the length of the offline block. An idea would be to apply a generalized classifier, trained on a healthy population, and test it on the SCI population. A similar approach has been developed recently in [74], for error-related potentials, and successfully applied online in SCI. Still, when testing such approaches or even individualized movement detectors in sensory complete SCI lesions an important question remains: how much is the performance affected when individuals with complete SCI, lacking sensory feedback, attempt to perform movements? Not only are the potentials altered during movement attempts, but also they are modulated by changes in sensory feedback [10, 75]. Furthermore, it is still necessary to evaluate whether the classifier would be invariant, or not, to different attention levels [30] and movement types. Additionally, the detector should still work even if the participants do not look at the target of interest. Such a generalization capability would greatly improve the functionality of the movement detector in real-life scenarios.

Finally, we believe it is fundamental to find strategies to improve the detection performance. For that, enriching the feature set with the EEG frequency domain (i.e. oscillations) could be beneficial, as well

as implementing deep learning methods provided that there is enough training data. For a more robust control, hybrid BCI approaches should also be considered [76]. Input signals could be provided from eye trackers or novel high-density EMG grids to better detect any residual movement activity [77]. Additionally, respiratory belts could also be used: very recently, it was shown that voluntary actions are coupled with breathing and that participants are more likely to initiate voluntary actions during the expiration phase [78]. The shared controllers of hybrid BCIs could cleverly make use of this information to improve the overall control performance.

5. Conclusion

We evaluated a novel experimental paradigm for upper-limb movement detection using low-frequency time-domain EEG signals. This approach is independent of external cues and of movement onset measurements, and is based on self-paced and natural reach-and-grasp movements. Additionally, the participants shifted their gaze towards the movement targets which closely resembles the natural goal-directed behaviour during reaching-and-grasping. Our classification approach exploited both MRCPs and activity generated from parietal and occipital areas. We were able to successfully detect movement online in an asynchronous classification scenario, and evaluated the presence of false positives under several conditions, including during a control oculomotor task. These findings contribute to the development of more intuitive and natural control strategies for BCIs for people without residual upper-limb movement function.

Data availability statement

The data that support the findings of this study are available upon reasonable request from the authors.


Acknowledgments

The authors would like to acknowledge the fruitful discussions with Catarina Lopes-Dias, Andreea I Sburlea and Lea Hehenberger. The authors thank Philipp Raggam and Michael Wimmer for their help during the EEG recordings. A special thanks to the volunteers which participated in the experiment in the atypical 2020. This work was supported by the ERC Consolidator Grant No. ERC-681231, Feel Your Reach.

ORCID iDs

Joana Pereira  <https://orcid.org/0000-0002-2032-8981>

Reinmar Kobler  <https://orcid.org/0000-0003-4007-279X>

Patrick Ofner  <https://orcid.org/0000-0001-7169-4300>

Andreas Schwarz  <https://orcid.org/0000-0002-3883-4989>

Gernot R Müller-Putz  <https://orcid.org/0000-0002-0087-3720>

References

- [1] Vidal J J 1973 Toward direct brain–computer communication *Annu. Rev. Biophys. Bioeng.* **2** 157–80
- [2] Wolpaw J R, Birbaumer N, McFarland D J, Pfurtscheller G and Vaughan T M 2002 Brain–computer interfaces for communication and control *Clin. Neurophysiol.* **113** 767–91
- [3] Millán J D R et al 2010 Combining brain–computer interfaces and assistive technologies: state-of-the-art and challenges *Front. Neurosci.* **4** 161
- [4] Müller-Putz G R, Scherer R, Pfurtscheller G and Rupp R 2005 EEG-based neuroprosthesis control: a step towards clinical practice *Neurosci. Lett.* **382** 169–74
- [5] Müller-Putz G R, Scherer R, Pfurtscheller G and Neuper C 2010 Temporal coding of brain patterns for direct limb control in humans *Front. Neurosci.* **4** 34
- [6] Kreilinger A, Kaiser V, Rohm M, Rupp R and Müller-Putz G R 2013 BCI and FES training of a spinal cord injured end-user to control a neuroprosthesis *Biomed. Tech.* **58** Suppl. 1
- [7] Mondini V, Kobler R J, Sburlea A I and Müller-Putz G R 2020 Continuous low-frequency EEG decoding of arm movement for closed-loop, natural control of a robotic arm *J. Neural. Eng.* **17** 046031
- [8] Pfurtscheller G and Aranibar A 1979 Evaluation of event-related desynchronization (ERD) preceding and following voluntary self-paced movement *Electroencephalogr. Clin. Neurophysiol.* **46** 138–46
- [9] Kornhuber H H and Deecke L 1964 Hirnpotentialänderungen beim Menschen vor und nach Willkürbewegungen und passiven Bewegungen des Menschen, dargestellt mit Magnetbandspeicherung und Rückwärtsanalyse *Pflügers Arch. Physiol.* **281** 52
- [10] Shibasaki H and Hallett M 2006 What is the Bereitschaftspotential? *Clin. Neurophysiol.* **117** 2341–56
- [11] Vuckovic A and Sepulveda F 2008 Delta band contribution in cue based single trial classification of real and imaginary wrist movements *Med. Biol. Eng. Comput.* **46** 529–39
- [12] Jochumsen M, Rovsing C, Rovsing H, Niazi I K, Dremstrup K and Kamavuako E N 2017 Classification of hand grasp kinetics and types using movement-related cortical potentials and EEG rhythms *Comput. Intell. Neurosci.* **2017** 7470864
- [13] Ofner P, Schwarz A, Pereira J, Müller-Putz G R and Zhang D 2017 Upper limb movements can be decoded from the time-domain of low-frequency EEG *PLoS One* **12** e0182578
- [14] Iturrate I, Chavarriaga R, Pereira M, Zhang H, Corbet T, Leeb R and Millán J D R 2018 Human EEG reveals distinct neural correlates of power and precision grasping types *Neuroimage* **181** 635–44
- [15] Schwarz A, Ofner P, Pereira J, Sburlea A I and Müller-Putz G R 2018 Decoding natural reach-and-grasp actions from human EEG *J. Neural. Eng.* **15** 016005
- [16] Schwarz A, Pereira J, Kobler R and Müller-Putz G R 2019 Unimanual and bimanual reach-and-grasp actions can be decoded from human EEG *IEEE Trans. Biomed. Eng.* **67** 1684–95
- [17] Farina D, Nascimento O F D, Lucas M-F and Doncarli C 2007 Optimization of wavelets for classification of movement-related cortical potentials generated by variation of force-related parameters *J. Neurosci. Methods* **162** 357–63
- [18] Gu Y, Dremstrup K and Farina D 2009 Single-trial discrimination of type and speed of wrist movements from EEG recordings *Clin. Neurophysiol.* **120** 1596–600
- [19] Fu Y, Xu B, Pei L and Li H 2011 Time domain features for relationship between speed and slow potentials activity during periodic movement and motor imagery at fast and slow for BCI *Procedia Environ. Sci.* **8** 498–505
- [20] Pereira J, Ofner P, Schwarz A, Sburlea A I and Müller-Putz G R 2017 EEG neural correlates of goal-directed movement intention *Neuroimage* **149** 129–40
- [21] Pereira J, Sburlea A I and Müller-Putz G R 2018 EEG patterns of self-paced movement imaginations towards externally-cued and internally-selected targets *Sci. Rep.* **8** 13394
- [22] Ofner P, Schwarz A, Pereira J, Wyss D, Wildburger R and Müller-Putz G R 2019 Attempted arm and hand movements can be decoded from low-frequency EEG from persons with spinal cord injury *Sci. Rep.* **9** 7134
- [23] Niazi I K, Jiang N, Tiberghien O, Nielsen J F, Dremstrup K and Farina D 2011 Detection of movement intention from single-trial movement-related cortical potentials *J. Neural. Eng.* **8** 066009
- [24] Lew E 2012 Detection of self-paced reaching movement intention from EEG signals *Front. Neuroeng.* **5** 13
- [25] Xu R, Jiang N, Lin C, Mrachacz-Kersting N, Dremstrup K and Farina D 2014 Enhanced low-latency detection of motor intention from EEG for closed-loop brain–computer interface applications *IEEE Trans. Biomed. Eng.* **61** 288–96
- [26] López-Larraz E, Montesano L, Gil-Agudo Á and Minguez J 2014 Continuous decoding of movement intention of upper limb self-initiated analytic movements from pre-movement EEG correlates *J. Neuroeng. Rehabil.* **11** 153
- [27] Sburlea A I, Montesano L and Minguez J 2015 Continuous detection of the self-initiated walking pre-movement state from EEG correlates without session-to-session recalibration *J. Neural. Eng.* **12** 036007
- [28] Walter W G, Cooper R, Aldridge V J, McCallum W C and Winter A L 1964 Contingent negative variation: an electric sign of sensori-motor association and expectancy in the human brain *Nature* **203** 380–4
- [29] Jankelowitz S and Colebatch J 2002 Movement-related potentials associated with self-paced, cued and imagined arm movements *Exp. Brain Res.* **147** 98–107
- [30] Aliakbarhosseiniabadi S, Kamavuako E N, Jiang N, Farina D and Mrachacz-Kersting N 2017 Influence of dual-tasking with different levels of attention diversion on characteristics of the movement-related cortical potential *Brain Res.* **1674** 10–19
- [31] Schwarz A, Höller M K, Pereira J, Ofner P and Müller-Putz G R 2020 Decoding hand movements from human EEG to control a robotic arm in a simulation environment *J. Neural. Eng.* **17** 036010
- [32] Katila T, Maniewski R, Poutanen T, Varpula T and Karp P J 1981 Magnetic fields produced by the human eye (invited) *J. Appl. Phys.* **52** 2565–71
- [33] Croft R J and Barry R J 2000 Removal of ocular artifact from the EEG: a review *Neurophysiol. Clin.* **30** 5–19
- [34] Kobler R J, Sburlea A I, Lopes-Dias C, Schwarz A, Hirata M and Müller-Putz G R 2020 Corneo-retinal-dipole and eyelid-related eye artefacts can be corrected offline and online in electroencephalographic and magnetoencephalographic signals *Neuroimage* **218** 117000
- [35] Kassner M, Patera W and Bulling A 2014 Pupil: an open source platform for pervasive eye tracking and mobile gaze-based interaction *Proc. 2014 ACM Int. Joint Conf. Pervasive and Ubiquitous Computing: Adjunct Publication* (New York: Association for Computing Machinery) pp 1151–60
- [36] Engbert R and Mergenthaler K 2006 Microsaccades are triggered by low retinal image slip *Proc. Natl Acad. Sci.* **103** 7192–7
- [37] Dimigen O, Sommer W, Hohlfeld A, Jacobs A M and Kliegl R 2011 Coregistration of eye movements and EEG in natural reading: analyses and review *J. Exp. Psychol. Gen.* **140** 552–72
- [38] Schlögl A and Brunner C 2008 BioSig: a free and open source software library for BCI research *Computer* **41** 44–50

- [39] Delorme A and Makeig S 2004 EEGLAB: an open source toolbox for analysis of single-trial EEG dynamics including independent component analysis *J. Neurosci. Methods* **134** 9–21
- [40] Tadel F, Baillet S, Mosher J C, Pantazis D and Leahy R M 2011 Brainstorm: a user-friendly application for MEG/EEG analysis *Comput. Intell. Neurosci.* **2011** 879716
- [41] Kobler R J, Sburlea A I, Mondini V and Müller-Putz G R 2019 HEAR to remove pops and drifts: the high-variance electrode artifact removal (HEAR) algorithm 2019 41st Annual Int. Conf. IEEE Engineering in Medicine and Biology Society (EMBC) pp 5150–5
- [42] Blankertz B, Lemm S, Treder M, Haufe S and Müller K-R 2011 Single-trial analysis and classification of ERP components—a tutorial *Neuroimage* **56** 814–25
- [43] Lotte F, Bougrain L, Cichocki A, Clerc M, Congedo M, Rakotomamonjy A and Yger F 2018 A review of classification algorithms for EEG-based brain–computer interfaces: a 10 year update *J. Neural. Eng.* **15** 031005
- [44] Kobler R J, Kolesnichenko E, Sburlea A I and Müller-Putz G R 2020 Distinct cortical networks for hand movement initiation and directional processing: an EEG study *Neuroimage* **220** 117076
- [45] Haufe S, Meinecke F, Görgen K, Dähne S, Haynes J-D, Blankertz B and Bießmann F 2014 On the interpretation of weight vectors of linear models in multivariate neuroimaging *Neuroimage* **87** 96–110
- [46] Lopes-Dias C, Sburlea A I and Müller-Putz G R 2019 Online asynchronous decoding of error-related potentials during the continuous control of a robot *Sci. Rep.* **9** 17596
- [47] Combrisson E and Jerbi K 2015 Exceeding chance level by chance: the caveat of theoretical chance levels in brain signal classification and statistical assessment of decoding accuracy *J. Neurosci. Methods* **250** 126–36
- [48] Nichols T E and Holmes A P 2002 Nonparametric permutation tests for functional neuroimaging: a primer with examples *Hum. Brain Mapp.* **15** 1–25
- [49] Blair R C and Karniski W 1993 An alternative method for significance testing of waveform difference potentials *Psychophysiology* **30** 518–24
- [50] Holmes A P, Blair R C, Watson J D and Ford I 1996 Nonparametric analysis of statistic images from functional mapping experiments *J. Cereb. Blood Flow Metab.* **16** 7–22
- [51] Gramfort A, Papadopoulos T, Olivi E and Clerc M 2010 OpenMEEG: opensource software for quasistatic bioelectromagnetics *Biomed. Eng.* **9** 45
- [52] Schäfer J and Strimmer K 2005 A shrinkage approach to large-scale covariance matrix estimation and implications for functional genomics *Stat. Appl. Genet. Mol. Biol.* **4** Article32
- [53] Pascual-Marqui R D 2002 Standardized low-resolution brain electromagnetic tomography (sLORETA): technical details *Methods Find. Exp. Clin. Pharmacol.* **24** 5–12
- [54] Skrandies W 1990 Global field power and topographic similarity *Brain Topogr.* **3** 137–41
- [55] Land M, Mennie N and Rusted J 1999 The roles of vision and eye movements in the control of activities of daily living *Perception* **28** 1311–28
- [56] Toma K, Matsuoka T, Immisch I, Mima T, Waldvogel D, Koshy B, Hanakawa T, Shill H and Hallett M 2002 Generators of movement-related cortical potentials: fMRI-constrained EEG dipole source analysis *Neuroimage* **17** 161–73
- [57] Stančák S A, Feige B, Lücking C H and Kristeva-Feige R 2000 Oscillatory cortical activity and movement-related potentials in proximal and distal movements *Clin. Neurophysiol.* **111** 636–50
- [58] Andersen R A 2011 Inferior parietal lobule function in spatial perception and visuomotor integration *Compr. Physiol.* (<https://doi.org/10.1002/cphy.cp010512>)
- [59] Connolly J D, Goodale M A, DeSouza J F X, Menon R S and Vilis T 2000 A comparison of frontoparietal fMRI activation during anti-saccades and anti-pointing *J. Neurophysiol.* **84** 1645–55
- [60] Rushworth M F S, Paus T and Sipila P K 2001 Attention systems and the organization of the human parietal cortex *NeuroImage* **13** 353
- [61] Musallam S 2004 Cognitive control signals for neural prosthetics *Science* **305** 258–62
- [62] Hadjidimitrakis K, Breveglieri R, Placenti G, Bosco A, Sabatini S P, Fattori P and Gribble P L 2011 Fix your eyes in the space you could reach: neurons in the macaque medial parietal cortex prefer gaze positions in peripersonal space *PLoS One* **6** e23335
- [63] Hadjidimitrakis K, Breveglieri R, Bosco A and Fattori P 2012 Three-dimensional eye position signals shape both peripersonal space and arm movement activity in the medial posterior parietal cortex *Front. Integr. Neurosci.* **6** 37
- [64] Sakata H, Taira M, Murata A and Mine S 1995 Neural mechanisms of visual guidance of hand action in the parietal cortex of the monkey *Cereb. Cortex* **5** 429–38
- [65] Ptak R and Müri R M 2013 The parietal cortex and saccade planning: lessons from human lesion studies *Front. Hum. Neurosci.* **7** 254
- [66] Scherberger H and Andersen R A 2007 Target selection signals for arm reaching in the posterior parietal cortex *J. Neurosci.* **27** 2001–12
- [67] Gallivan J P, Chapman C S, Gale D J, Flanagan J R and Culham J C 2019 Selective modulation of early visual cortical activity by movement intention *Cereb. Cortex* **29** 4662–78
- [68] Muckli L and Petro L S 2013 Network interactions: non-geniculate input to V1 *Curr. Opin. Neurobiol.* **23** 195–201
- [69] Niazi I K, Mrachacz-Kersting N, Jiang N, Dremstrup K and Farina D 2012 Peripheral electrical stimulation triggered by self-paced detection of motor intention enhances motor evoked potentials *IEEE Trans. Neural. Syst. Rehabil. Eng.* **20** 595–604
- [70] Martínez-Expósito A, Ibáñez J, Resquín F and Pons J L 2017 Task influence on motor-related cortical signals: comparison between upper and lower limb coordinated and analytic movements *Converging Clinical and Engineering Research on Neurorehabilitation II Biosystems & Biorobotics* (Berlin: Springer) pp 1139–43
- [71] Jochumsen M, Niazi I K, Mrachacz-Kersting N, Farina D and Dremstrup K 2013 Detection and classification of movement-related cortical potentials associated with task force and speed *J. Neural. Eng.* **10** 056015
- [72] Jochumsen M, Niazi I K, Taylor D, Farina D and Dremstrup K 2015 Detecting and classifying movement-related cortical potentials associated with hand movements in healthy subjects and stroke patients from single-electrode, single-trial EEG *J. Neural. Eng.* **12** 056013
- [73] Schultze-Kraft M, Birman D, Rusconi M, Allefeld C, Görgen K, Dähne S, Blankertz B and Haynes J-D 2016 The point of no return in vetoing self-initiated movements *Proc. Natl Acad. Sci.* **113** 1080–5
- [74] Lopes Dias C et al 2020 Online asynchronous detection of error-related potentials in participants with a spinal cord injury by adapting a pre-trained generic classifier *J. Neural. Eng.* **18** 4
- [75] Galán F, Baker M R, Alter K and Baker S N 2015 Degraded EEG decoding of wrist movements in absence of kinaesthetic feedback *Hum. Brain Mapp.* **36** 643–54
- [76] Müller-Putz G R et al 2011 Tools for brain–computer interaction: a general concept for a hybrid BCI *Front. Neuroinform.* **5** 30
- [77] Ting J E, Del Vecchio A, Sarma D, Colachis S C, Annetta N V, Collinger J L, Farina D and Weber D J 2021 Sensing and decoding the neural drive to paralyzed muscles during attempted movements of a person with tetraplegia using a sleeve array *medRxiv* (available at: www.medrxiv.org/content/10.1101/2021.02.24.21250962v1.abstract)
- [78] Park H-D, Barnoud C, Trang H, Kannape O A, Schaller K and Blanke O 2020 Breathing is coupled with voluntary action and the cortical readiness potential *Nat. Commun.* **11** 289